CENTRO DE INVESTIGACIONES
EN OPTICA, A.C.

“OPTICAL PROPERTIES OF BLUE PHOSPHORENE CONSIDERING MANY-BODY EFFECTS”

Tesis que para obtener el grado de Maestro en Ciencias (Óptica)

Presenta: Juan José Nava Soto

Director de Tesis: Dr. Norberto Arzate Plata

Versión Definitiva. Incluye cambios sugeridos por revisores

León · Guanajuato · México
Agosto de 2023

En ella estaba la vida, y la vida era la luz de los hombres. La luz brilla en las tinieblas, y las tinieblas no la recibieron. Apareció un hombre enviado por Dios, que se llamaba Juan. Vino como testigo, para dar testimonio de la luz, para que todos creyeran por medio de él. Él no era la luz, sino el testigo de la luz. La Palabra era la luz verdadera que, al venir a este mundo, ilumina a todo hombre.

El evangelio según San Juan, I, 4-9.

Y al hablar de fenómenos, me refiero particularmente al de la luz, que, en lugar de mostrarlo, o de demostrarlo, nos oculta el semblante de las cosas gracias al maquillaje de los siete colores del espectro que se resumen en uno y nos dejan en blanco. Esto es: ignorantes solemnes de todo lo que ocurre en el mundo...

Juan José Arreola, *Inventario*, p. 64.

Acknowledgements

Words cannot express my gratitude to professor Norberto Arzate Plata for his invaluable patience and feedback in these two years working with him.

Special thanks to my defense committee, Dr. Laura Rosales Zárate and Peter Rodríguez Kessler, who generously provided knowledge and expertise.

Additionally, this endeavor would not have been possible without the support from CONACYT for the scholarship 2021-000018-02NACF-20580, which permitted me to develop this project completely.

I am also grateful to professor Mario Ruiz Berganza for his editing help and advice writing this thesis.

I would be remiss in not mentioning my family, especially my parents and sister. Their belief in me has kept my motivation high during this process.

Finally, I would like to acknowledge the group of Optical Properties of Interfaces, Nanosystems and Metamaterials (Propiedades Ópticas de Superficies, Interfaces, Nanosistemas y Metamateriales (PROSINyM)), for the facilities in using the computational resources. The numerical study was partially supported by CONACYT trough the project with identification number A1-S-9410.

Abstract

Since the discovery of black phosphorene (a monolayer of bulk black phosphorus), new 2D allotropes of phosphorus have been predicted and studied due to their interesting properties. Some possible applications of these phosphorene structures could be in photovoltaic cells, gas sensors and rechargeable batteries. In particular, blue phosphorene is characterized by having a hexagonal structure, and thus, an isotropic optical response on the plane of the layer structure. The electronic band structure of blue phosphorene was obtained by using Density Functional Theory within the Generalized Gradient Approximation. It is observed, based on its band structure, that blue phosphorene shows a semiconducting nature, with an indirect band gap. The energy corrections to the bands were calculated in a specific set of $\mathbf{k}$ points within the irreducible Brillouin zone by employing the GW approximation and the complete quasiparticle band structure was determined by using maximally-localized Wannier functions. The comparison between Generalized Gradient Approximation and GW calculated band structures shows that there are significant differences, which demonstrates the importance of performing quasiparticle corrections. In general, neither the calculation of the optical spectrum in the independent-particle approach nor the calculation using the the quasiparticle energies obtained in a GW correction match correctly the experimental data of the absorption of the materials. Therefore, the optical response including excitonic effects (electron-hole interactions) has to be calculated. For that, the excitonic spectrum is obtained and compared with both the independent-particle and GW optical response.

Contents

List of Figures

List of Tables

Chapter 1

Introduction

In this first chapter, I will present, as naturally as I can, a logical succession of the ideas that I consider important to know in order to comprehend the course of some electronic structure methods, that is, the description of electrons in matter. An accurate description permits us to calculate the fundamental properties of atomic crystals, as in the case of this project, where the main goal was to obtain the optical properties of blue phosphorene using first principles methods. Then, a review of the most important parts of the works where graphene was first studied is presented. It was the first two dimensional material and it is important to know the interesting properties that graphene posses. Finally, a complete description of blue phosphore, the object of study in this work, is also made.

Some prior results are directly related to the development of this work and are fundamental to understand the methodological proceedings and the importance of conducting this specific investigation; some others are indirectly related, as one can see after a first reading.

Many works have been omitted due to the introductory character of this part of the text. The goal behind the analysis of the more important ones is to understand, to clarify and to present a chronological review of why and how scientific thought has been conducted and has arrived to the present paradigms in electronic structure calculations, as could be the Density Functional Theory.

In some parts, I present exact quotes from the original works, mainly in

order to appreciate the thoughts of the author as written in his text, and to present the ideas in a clearer way than I would be able to do myself; in other cases, the comments of some authors about previous works of others are also highlighted.

1.1 The beginnings of quantum theory

For the sake of completeness, a revision of some of the fundamental works on quantum mechanics are presented. Even though the language used to present the results may seem obscure, in some sense (which can also be due to the translation of many of them, originally written in German or French). Here, I will present the main ideas behind those works.

In 1900, Max Planck published a summary [1] that was intended to explain the recent law of distribution of radiation obtained by him. He said that, based on the laws of electromagnetic radiation, thermodynamics and probability calculus, he had been able to come to such deduction. However, he did not want to pay attention to the hard evidence but to clearly explain the main results. He presented the new constant of nature called h, whose value was obtained by Planck that year and was equal to 6.55×10^{-27}, among other physical constants such as Avogrado's constant. He explained that a chosen energy element ϵ for a given resonator, vibrating inside a diathermic medium with reflecting walls, must be proportional to its frequency ν and to constant h, now called Planck's constant. He said that, as he had mentioned in other occasions, *"the energy of the radiation is completely 'randomly' distributed over the various partial vibrations present in the radiation"*. With this, quantum theory could be considered to have originated, being h the fundamental quantum of action.

A few years later, Einstein [2] described, in terms of energy quanta, the photoelectric effect, which had been identified years before: *"The usual idea that the energy of light is continuously distributed over the space through which it travels meets with especially great difficulties when one tries to explain photo-electric phenomena..."*. He referred to other phenomena and to the importance of having a new description of light: *"...it seems to me that the observations on "black-body radiation", photoluminescence, the production of cathode rays by ultraviolet light and other phenomena involving the emission or conversion of light can be better understood on the assumption*

that the energy of light is distributed discontinuously in space. According to the assumption considered here, when a light ray starting from a point is propagated, the energy is not continuously distributed over an ever increasing volume, but it consists of a finite number of energy quanta, localised in space, which move without being divided and which can be absorbed or emitted only as a whole...".

The next important work is the one published by Niels Bohr in 1913, which is divided into three different parts. In the first of them [3], Bohr elucidated about the way of describing the atoms, i.e., to propose an atomic model which could describe matter at its best. At that time, the atomic models of Rutherford and Thomson were under investigation; both were incorrect considering the theoretical point of view (in the case of Rutherford's model) and the experimental (in the case of Thomson's model). Bohr identified the inadequacy of using the classical theory of electrodynamics to describe an atom and used the previous results obtained by Planck and Einstein to propose a series of different stable states. The electrons in these states can be described using ordinary mechanics, but the passing between different states is related to the emission of a light quantum of homogeneous radiation whose energy is described with Planck's theory; this is how he was able to explain the line spectra of the elements.

In the second part [4], guided by the hypothesis of the quantization of the electrons angular momentum (in multiples of $h/2\pi$ or $\hbar$) of the atom and the relations obtained in the first part, he tried to indicate the different electron configurations that would be expected for different atoms. Even though some assumptions are fundamentally incorrect, he was able to adequately explain some properties of the first four elements of the periodic table.

Lastly, in the third part [5], Bohr treated the chemical bond considering atoms composed of a nucleus and surrounding electrons that interact to form a molecule. The concluding remarks are very important. The author took the idea proposed by Planck of the monochromatic vibrators, responsible of the black-body radiation. He assumed that they were the atoms which were responsible for the discrete transitions, due to the quantization of the different energy levels of the electrons.

A few years later, in his PhD thesis, L. De Broglie [6] derives his famous relation between the movement of a particle at a specific velocity and the wavelength related to it. This derivation is not as straightforward as one

would think at first; he uses lots of previous works from the field of mechanics and relativity, as well as recent quantum papers. This subtle idea of an intrinsic wave nature present in matter is one of the principles on which quantum mechanics is built.

The works presented by Heisenberg [7], by Born and Jordan [8], and by the three of them together [9] deal with the theoretical treatment of quantum mechanics as an analogous to the classical mechanics formulation. The necessity of expressing observable quantities as matrices arose in Heisenberg's paper, and the commutation relation for position and momentum appeared to be different from zero (equal to $i\hbar$), referred to as the "stronger quantum condition", in the second work. In the third one, the matrix formulation was taken a step forward and applied to different cases in order to demonstrate that the approach is correct; they used an approach closely related to the prevailing classical theory, finding adequate expressions and a direct connection.

The final important work to be reviewed here is that of Schrödinger's [10]. Following De Broglie's proposition, the author stated that, maybe, *"the material points consist, or are nothing but, wave-systems"*. He was doubtful about this idea, because *"it does not offer an explanation of why such wave-systems seem to be realized in nature"*. However, Schrödinger's intuition took him to an analogy between the ideas applied to geometrical optics and how these were unable to explain some physical optics phenomena, such as diffraction; the uncertainty of the applicability of ordinary mechanics to *"micro-mechanical wave-phenomena"* came later. Then, he presented his famous wave-equation and applied it to solve the problem of the hydrogen atom, getting a set of discrete energy levels, in the same way as Bohr had obtained with his model. What is more satisfying is that, according to the author, this undulatory mechanics description is in complete agreement with that of matrices proposed by Born and others. At the end, Schrödinger tried to relate the physical significance of the wavefunction (the solution of the wave-equation) to the intensity of light emitted by atoms. This formal ondulatory description of matter paved the wave for the application of quantum mechanics to many other physical phenomena.

Finally, I would like to mention that other very important works, carried out at the same time as the previous ones, were those that dealt exclusively with electrons. For example, the way of describing their behavior under different

conditions, as the Fermi-Dirac statistical distribution, and the explanation of the electron's spin and its direct consequences, were also fundamental to the development of a complete quantum theory.

1.2 Solid-state physics considerations

The ideas developed in quantum theory, in particular those described in section 1.1, were groundbreaking. This is considered as a clear example of a scientific revolution by Thomas Kuhn [11]. It is important to present how these new fundamental ideas were applied to what is called solid-state physics, whose main interest is the understanding of the behavior of electrons in crystalline materials.

Felix Bloch [12], was interested in explaining how electrons move trough a crystal lattice. He assumed that the interactions of such electrons with the crystal were due to an effective periodic potential with the periodicity of the crystal lattice. Therefore, the problem is thus simplified to how an independent electron obeys the one electron Schrödinger's equation inside a crystal. Bloch concluded that one could study the whole crystalline lattice by just considereding one unit cell, due to its symmetry and periodic boundary conditions. What is now called Bloch's theorem is a mathematical description that helps us to express the solution of this Schrödinger's equation (the electron's wavefunction) as a plane wave modulated by a periodic function with lattice periodicity. Nonetheless, it does not give us an explicit form of the solution, but confine the possibilities to those of this kind, which is very helpful. The description of the reciprocal lattice appears naturally in this formulation as "Fourier dual" of the crystal or direct lattice.

A. H. Wilson described the consequences of the Bloch theorem [13], obtained and described by Brillouin [14] and by Kronig and Penney [15] on the problem of one electron moving in a one-dimensional periodic potential as: *"it appears that the energy levels break up into a number of bands of allowed energies, separated by bands of disallowed energies"*, and that is what is now called the band theory. He explained the resulting energy bands in solids using the nearly free electron model and the tightly bound electron model. He tried to relate the characteristics of the electronic structure of a given element to its nature as a metal or as a semiconductor and in the last pages, he already uses the categories of semiconductor and insulator as we use them today.

It is important to mention that the problem of the electrons moving in crystals is of course a many-body problem. P.A.M Dirac, in 1929 [16], took into account the interaction among electrons through the exchange interaction, which arises owing to the indistinguishability of electrons from another; two electrons can exchange places, and the possibility of this gives rise to the conclusion that it is a pure quantum mechanical effect. He considered the permutation of electrons as an operator, acting on the wavefunction in a many-body problem. A conclusion can be directly drawn: the exchange is an essential degeneracy between all the similar particles, because the Hamiltonian is invariant under these permutations.

In the same sense, another important effect in matter is the correlation between electrons. In some way, we could describe it as the influence felt by one electron due to the presence of the other ones. Wigner studied the correlation of electrons in sodium in 1934 [17]; he considered a new term, due to correlation of electrons with antiparallel spin, in the Hartree-Fock formulation (reviewed to some extent in the next subsection). In this way, he made a generalization of the method, allowing for these interactions, and considering a correction in the total energy, called "correlation energy" by him. Wigner was able, within some approximations, to calculate the energy of the ground state, to determine the lattice parameter and the binding energy, and to compare these two quantities with values obtained experimentally in that time. Lastly, he concluded by saying that the correlation energy is important in matters of paramagnetism, ferromagnetism and lattice energy. Even though there were many approximations in the calculation, the inclusion of correlation and the consideration of the important role that it plays in determining the crystal structure are of great recognition.

1.3 Efforts made in computing electronic structure

After having revised the key ideas that were used to formulate a theoretical description of electrons in matter, now it is important to review some of the first works in which the calculation of the electronic structure was the main objective. The fundamental basis for understanding materials and phenomena ultimately rests upon understanding electronic structure; the modern *ab initio* calculations were developed trying to reach this objective too.

1.3.1 Early attempts

L.H. Thomas [18] had the intention of giving a method to determine approximated electric fields inside a heavy atom. He considered (1) that relativistic corrections can be neglected, (2) that the effective potential felt by an electron only depends on the distance from the nucleus, (3) that there is a uniform distribution of electrons in phase space (two per unit cell), and (4) that the potential is determined by the nuclear charge and the distribution of electrons. The most remarkable contribution is that he was able to relate the momentum of the electrons to the charge density; so, in principle, it is possible to obtain one from the other.

Unfortunately, Fermi's related work [19] was not available to compare the expressions obtained by both, but, due to that almost the same methodology was derived independently and presented the same year, the complete model is known nowadays as the Thomas-Fermi model.

In 1930, at a time when the quantum theoretical methods were not practicable when dealing with systems having many electrons, Dirac focused on the Thomas-Fermi model. It was simpler though rougher one. He pointed out that such a method is provided by *"Thomas' atomic model, in which the electrons are regarded as forming a perfect gas satisfying the Fermi statistics and occupying the region of phase space of lowest energy. This region of phase space is assumed to be saturated, with two electrons with opposite spins in each volume* $(2\pi h)^3$*, and the remainder is assumed to be empty"*. He derived a new equation with an added term as a correction for the density on account for the exchange effects [20]. Due to this, the complete model is referred by some authors as the Thomas-Fermi-Dirac model.

In the work of Dirac, in which he treated exchange as a permutation ([16]), Hartree's self-consistent field method is mentioned as a breakthrough in considering orbitals of electrons not as an individual orbit, but as a quantum state, represented by a three dimensional wavefunction. He also said that the method, apparently, does not have a theoretical justification, but it matches experiments very well. In the first of four parts [21], Hartree explained that *"Schrodinger's suggestion concerning the interpretation of* ψ*,"* the wavefunction, *"affords a hope that it may be possible to consider the internal field of the atom as being due to the distribution of charge given by the characteristic functions for the core electrons; we may, in fact, attempt to find a field of*

force such that the total distribution of charge, given by the characteristic functions in this field, reproduces the field". The general idea is to determine the wavefunction for a *"non-Coulombic central field of force"* whose potential is given.

In order to eliminate several constants from the equations, Hartree introduced atomic units for the first time [21]; which roughly speaking, constitute a new set of units that uses characteristic quantities of the hydrogen atom. For example, the length unit is defined as the Bohr radius of the hydrogen atom, the charge unit is the electron charge, and the mass unit is the electron mass. He defined an energy unit, which is twice the ionisation energy of the hydrogen atom, that is now known as *1 Hartree* or *1 Ha*. He used the classical $\hbar$ as unit of action, and also defined a unit for time.

In the second part [22], the self-consistent method is described as follows:

"Consider an atom such as the neutral atom of an alkali metal, consisting of closed n_k groups and a series electron. The potential v for the series electron is that of the field of the centrally symmetrical distribution of charge of the closed groups; but just as in the theory of the hydrogen atom the field acting on the electron is that of the nucleus only, not that of the nucleus and its own distributed charge, so here the field for a core electron is the total field of the nucleus and all the closed groups, less its own contribution to that field. Now except for an electron with $l = 0$, its own contribution to the field is not centrally symmetrical, so that it would seem that the assumption of a central field is not applicable to it... It is just here that we meet the most serious doubts concerning the replacement of the actual many-body problem by a one-body problem with a central field for each electron, even as a first approximation".

Evidently, a field felt by an specific electron is that of the nucleus, plus that of the closed group of electrons surrounding that nucleus, without considering the field contribution of this specific electron.

The last remark is referred to the plausible doubt of applying this method to non centrally symmetrical distribution of charge, that is, in cases where the orbital angular momentum number (l) of the electrons is different from zero

"For numerical work we have to start from a field which will be called the 'initial field'; for each n_k corresponding to a group of core electrons the field is corrected, as explained above, for the fact that the distributed charge of an

electron must be omitted in finding the field acting on it, and for the field so corrected the part of the solution of the wave equation depending on r is found by the methods given in I; then from the solutions for all groups of core electrons a distribution of charge can be calculated (if the n_k groups are all complete, this distribution of charge will be centrally symmetrical), and then the field of the nucleus and this distribution of charge can be found; this may be called the 'final field'".

This process is shown in diagrammatic form in Figure 1.1

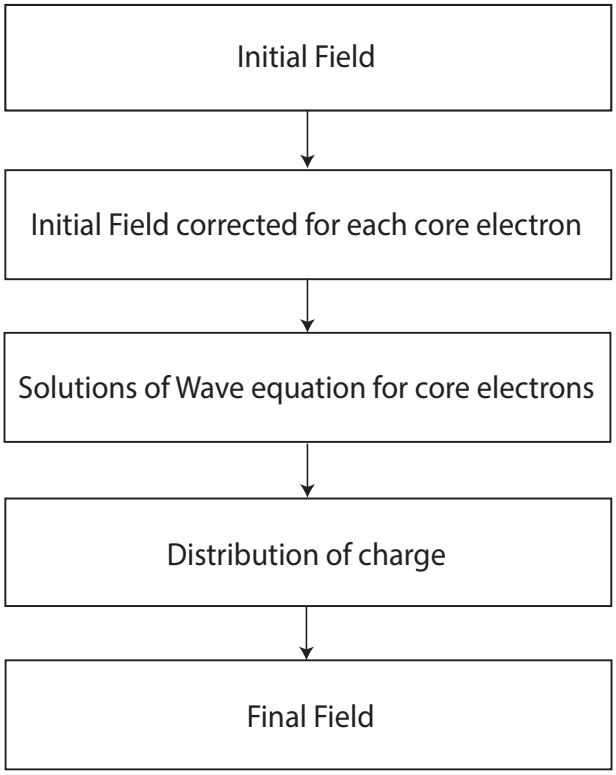

Figure 1.1: Flow chart for applying the self-consistent field method. Taken from the second paper of Hartree's work *"The wave Mechanics of an Atom with a Non-Coulombic Central Field"* [22].

If the final field is the same as the initial field, it is called a "self-consistent field", and is characteristic of the particular atom in particular state. Hartree

calculated the ground state energy of helium, rubidium, sodium and chlorine using his method, giving results in accordance with experiments.

Two years after, the work of Dirac ([20]) was presented, which helps us to put in context the previous work: *"The method of the self-consistent field has recently been established on a very much better theoretical basis in a paper by Fock,"* ([23]) *"which shows how one can take into account the exchange phenomena between the equivalent electrons. Fock shows that if one takes the best approximation to the many-dimensional wave function that is of the form of a product of a number of three-dimensional wave functions, one for each electron, then the three-dimensional wave functions will satisfy just Hartree's equations. In this way a theoretical justification for Hartree's method is obtained. The exclusion principle of Pauli, however, requires that the wave function representing a number of electrons shall always be antisymmetrical. One would therefore expect to get a better approximation if one first made the product of a number of three-dimensional wave functions antisymmetrical, by applying permutations and taking a linear combination, and then made it approach as closely as possible to the accurate many-dimensional wave function. The three-dimensional wave functions will then, as found by Fock, satisfy equations somewhat different from Hartree's, containing extra terms which may be considered as representing the exchange phenomena".* Dirac contribution in this case was to obtain Fock's equivalent equations but, in considering the spin of the electron, adding in the derivation a new variable in the description of the wavefunction of the problem, generalizing the theoretical description.

1.3.2 The foundations of Density Functional Theory

Years passed, and it was not until 1964 that the work of Hohenberg and Kohn [24] was published. This is considered as one of the fundamental works that gave birth to the modern Density Functional Theory (DFT). [1]

In Hohenberg-Kohn (HK) work [24], the introduction asserts in giving some context:

"The point of view has been, in general, to regard the electrons as similar to a collection of noninteracting particles with the important additional concept of

[1] Readers are also referred to Appendix A for the mathematical description of a functional and to identify the notation used here and in the next chapter.

collective excitations. On the other hand, there has been in existence since the 1920's a different approach, represented by the Thomas-Fermi method and its refinements, in which the electronic density $n(r)$ plays a central role..."

The two HK theorems are the most important part of the paper. They considered that the ground state was not degenerate and in their own words, the first one is presented [24] and proven by *reductio ad absurdum*:

"We denote the electronic density in the ground state by $n(r) \equiv (\Phi\psi^*(r)\psi(r)\Phi)$, which is clearly a functional of $v(r)$".

Conversely, they stated that

"...$v(r)$ is (to within a constant) a unique functional of $n(r)$; since, in turn, $v(r)$ fixes H we see that the full many-particle ground state is a unique functional of $n(r)$". Where H is the hamiltonian of the system.

The second one is presented as the variational principle as [24]:

"If $F[n]$ were a known and sufficiently simple functional of n, the problem of determining the ground-state energy and density in a given external potential would be rather easy since it requires merely the minimization of a functional of the three-dimensional density function. The major part of the complexities of the many electron problems are associated with the determination of the universal functional $F[n]$".

Given this theoretical description, not really simple but presented in a very condensed manner, the next step is to find a way to determine this universal functional that, thanks to the demonstrations, does exist. The description of electronic structure limits to minimizing this functional.

The other DFT foundational work deals with this last consideration and was presented by Kohn and Sham in 1965 [25]. They began saying that:

"... we use the formalism of Hohenberg and Kohn to carry this approach further and we obtain a set of self-consistent equations which include, in an approximate way, exchange and correlation effects..." They require only a knowledge of the true chemical potential, $\mu_h(n)$, of a homogeneous interacting electron gas as a function of the density n. *"We derive two alternative sets of equations... which are analogous, respectively, to the conventional Hartree and Hartree-Fock equations, and, although they also include correlation effects, they are no more difficult to solve".*

Moreover, they showed that the description of the ground-state of a system can also be given in considering finite temperature. The expressions for the low-temperature specific heat, for metals and alloys, and the spin susceptibility were obtained.

The last note is essential [25]:

"We should like to point out that it is possible, formally, to replace the many-electron problem by an exactly equivalent set of self-consistent one-electron equations."

They stated that it is accomplished quite simply by using the expression for the universal functional on the density in the variational principle. The universal functional is given as $F[n] \equiv T_s[n]+E_{xc}[n]$, where $T_s[n]$ is the kinetic energy of a system of non-interacting electrons with density $n(r)$ and $E_{xc}[n]$ is the exchange and correlation energy functional of a interacting system with density $n(r)$.

Then the main task is to know the explicit form of the exchange-correlation energy functional, which includes the many-body effects. Knowing this, one can obtain the total energy for the ground state.

A formulation of the Kohn-Sham equations is given in the next chapter (section 2.2), using rigorous mathematical expressions and a diagram to clarify the process. Evidently, with this brief description and presentation of some extracts of original works, one can get an idea of what a powerful tools these equations are to obtain electronic structure.

1.4 Two dimensional materials

Two dimensional or 2D materials are one of the main active areas of research in material science. They could be described as materials that have few atomic layers where the in-plane interatomic interactions is much stronger than those that take place in the perpendicular direction. The main reason for the great interest in this kind of materials is that their properties are completely different from the bulk structure, giving place to an interesting object of study that can be useful in the development of new technologies [26].

The beginning of 2D materials can be traced to the work directed by K.S.

Novoselov, A.K. Geim and colaborators in 2004 [27]. They synthesized graphene successfully for the first time and analyzed its properties. In this work, graphene was first described as *"monocrystallyne graphitic films of a few atoms thick but nonetheless stable under ambient conditions"*. They also called it *"...a naturally occurring two-dimensional (2D) material referred to as few-layer graphene"*. They explained that *"Graphene is the name given to a single layer of carbon atoms densely packed into a benzene-ring structure"*.The graphene layers were obtained using mechanical exfoliation or repeated peeling of graphite.

Novoselov *et al.* reported the observation of electric-field effect in few layers graphene. They obtained the plots for the behavior of resistivity, conductivity and Hall coefficient as a function of gate voltage. In particular, they obtained high carrier mobilities. They concluded that graphene may be the best possible metal for metallic transistor applications as well as in ballistic transport. They finished by saying that *"... nontransistor applications of this atomically thin material ultimately may prove the most exciting"*.

A year after, the same group studied some other 2D materials [28]. Using mechanical cleavage, they synthesized single layers of boron nitride, graphite and transition metal dichalcogenides, which were stable under ambient conditions and posses high crystal quality and continuity on a macroscopic scale. In some sense, the research on 2D materials beyond graphene was initiated then.

Some description regarding the methods is important to understand the difficult task that it was to characterize 2D materials experimentally. Novoselov *et al.* listed some features of the cleavage technique [28]:

"1. Monolayers are in a great minority among accompanying thicker flakes."

"2. Unlike nanotubes, 2D crystals have no clear signatures in transmission electron microscopy."

"3. Monolayers are completely transparent to visible light and cannot be seen in an optical microscope on most substrates (e.g., on glass or metals). AFM is currently the only method that allows definitive identification of single-layer crystals, but it has a very low throughput (especially for the case of the high-resolution imaging required), and in practice it would be impossible to find cleaved 2D crystallites by scanning surfaces at random."

"4. It was not obvious that isolated atomic planes could survive without their parent crystals."

The last important work to be reviewed in the topic is that presented by the research group in the same year. There, the linear dispersion relation (energy as a function of the wavevector) for electrons and holes in graphene is proved experimentally [29] and, when compared with previous theoretical results ([30]), the inferred electronic spectrum it is well matched, showing, at the Brillouin zone boundary, the shape of two cones (a valence cone and a conduction one) that touch each other at their tips, which means that, this material has a zero band gap.

This important result implies that the rest mass of the electrons is zero, and that is the reason why one refers to this kind of electrons as massless fermions or Dirac fermions, because it is necessary to use the Dirac equation for massless relativistic fermions instead of that of Schrödinger for calculations. However, the cyclotron effective mass (the mass that would be measured if one performs a cyclotron resonance frequency experiment of the material [31]) is not zero and, in measuring this quantity, they obtained that the velocity at which the charge carriers move in graphene is approximately 1/300 times the velocity of light in vacuum.

The measured quantum Hall effect in graphene was also unusual. This effect can be defined as a quantization of the Hall resistance in a two-dimensional electron system subject to a strong magnetic field. In the case of graphene, the quantization of the conductivity do not occur at integer values but at half-integers. On the contrary, for two-layered graphene the quantization returns to the expected integer changes. The qualitative transition between graphene and its two-layer counterpart is a consequence of the nature of fermions in graphene, which are described as massless Dirac particles.

All of this, in some sense, explains why graphene is such an interesting material to study, why the research related to 2D materials dramatically increased in the years after its discovery [26], and why Geim and Novoselov won the Nobel prize in Physics in 2010.

Evidently, many new proposals for stable 2D materials have been made, and a lot of studies have been conducted to characterize them; some examples could be the transition metal dichalcogenides [32] and boron nitride [33], and others were predicted just a few years ago, as black phosphorene [34].

The possible applications of these materials are varied, depending on their specific properties. Some of them have been proposed for chemical sensing [35], as saturable absorbers in laser technology [36], for fabricating photovoltaic cells [37], for quantum information devices [38], among other possible applications. Their potential usage also depends on the characterization and fabrication techniques, that is why many new developments have been proposed in those areas, trying to reduce the costs of synthesizing them, and making it competitive for the industry to produce them in mass.

1.5 Blue phosphorene

Phosphorus presents many allotropes, that have been studied for more than a century. Some of them could be the black, red, white and purple phosphorus [39, 40]. The color of the allotrope relates directly with its fundamental energy band gap value since it could be characterized by the way it absorbs light.

A few years ago, it was predicted that thin black phosphorus layers were stable in environmental temperature and due to the similarity with graphene it was called phosphorene. This allotrope presents a non-planar structure [41] and, being a semiconductor, posses interesting electronical properties, as a high carrier mobility [42]. Now, it has received the name of black phosphorene, because many new 2D phosphorus allotropes have been predicted and, as in the case of bulk ones, characterized by the way they absorb light.

The polymorphism that some elements present remains as a interesting topic. Crystalline structures are modified when the temperature or the pressure of the environment change but the specific reason for a particular atomic arrangement is still under debate [43]. In the case of phosphorus, very recently it was demonstrated that the black phosphorene structure could be modified, giving place to a more symmetrical hexagonal structure (translocating some phosphorus atoms) that was named blue phosphorene [41]. It was also demonstrated that this structure was practically as stable as the black phosphorene one [44]. This hexagonal structure is such as that of graphene but the difference being that the blue phosphorene monolayer is non-planar [45]. Among many other differences that one should expect to observe between the two crystalline structures is that black phosphorene is a direct band gap semiconductor while blue phosphorene is an indirect band gap semiconductor

[46].

1.5.1 Structure

The hexagonal structure is what differentiates blue phosphorene among the others phosphorenes. In Figure 1.2, there is a comparison between a synthesized monolayer of blue phosphorene (deposited over a gold substrate) and obtained with the Scanning Tunneling Microscope (STM) and the theoretical prediction obtained using a simulation.

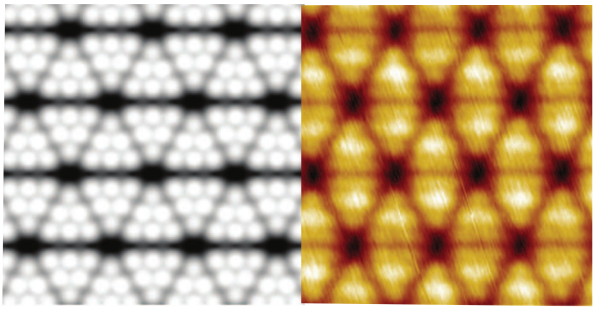

(a) (b)

Figure 1.2: (a) Theoretical array of atoms predicted by a simulation scheme developed by [47]. (b) STM image obtained by the same authors.

As it was mention previously, the blue phosphorene structure resembles that of graphene, but with the difference that the atoms in the unit cell are not on the same atomic plane. With this information, it was determined that blue phosphorene belongs to the point group of symmetry ($P\bar{3}m1$, #164) [48]. In Figure 1.3, some schematics diagrams of the structure are shown.

For describing an hexagonal crystal we use the set of primitive lattice vectors, whose magnitude is proportional to the lattice constants a and c

$$\mathbf{a_1} = (1, 0, 0)\, a, \tag{1.1}$$

$$\mathbf{a_2} = \left(\frac{1}{2}, \frac{\sqrt{3}}{2}, 0\right) a, \tag{1.2}$$

$$\mathbf{a_3} = (0, 0, 1)\, c. \tag{1.3}$$

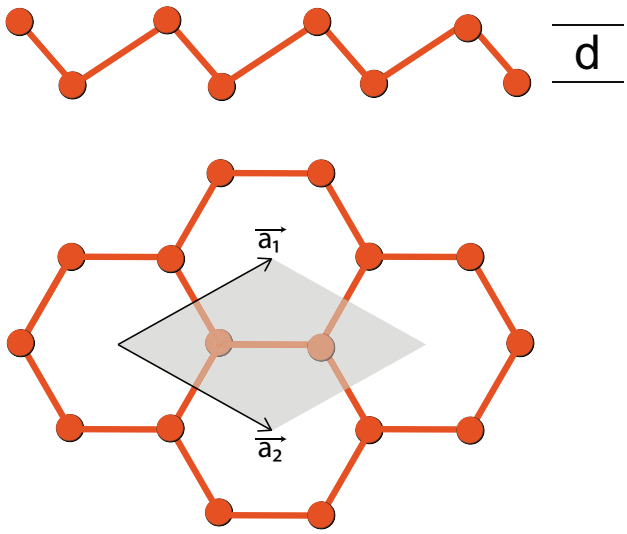

Figure 1.3: Side and upper view of the crystalline structure of blue phosphorene. d represents the distance between the atomic planes of the atoms inside the unit cell, $\mathbf{a_1}$ and $\mathbf{a_2}$ are the primitive vectors and the shaded area represents the unit cell. Taken from [49].

The primitive lattice vectors set for the reciprocal space can be written as

$$\mathbf{b_1} = \left(1, -\frac{1}{\sqrt{3}}, 0\right)\frac{2\pi}{a}, \tag{1.4}$$

$$\mathbf{b_2} = \left(0, \frac{2}{\sqrt{3}}, 0\right)\frac{2\pi}{a}, \tag{1.5}$$

$$\mathbf{b_3} = (0, 0, 1)\,\frac{2\pi}{c}. \tag{1.6}$$

Using the latter, it is possible to construct the first Brillouin zone, which is just the hexagonal lattice in real space but rotated sixty degrees, as shown in Figure 1.4. The importance of the reciprocal space comes from the fact that all possible eigenstates are specified by $\mathbf{k}$ within any primitive cell of the periodic lattice in this space. However, the first Brillouin zone is the cell of choice in which the optical physical process such as the excitations are referred to.

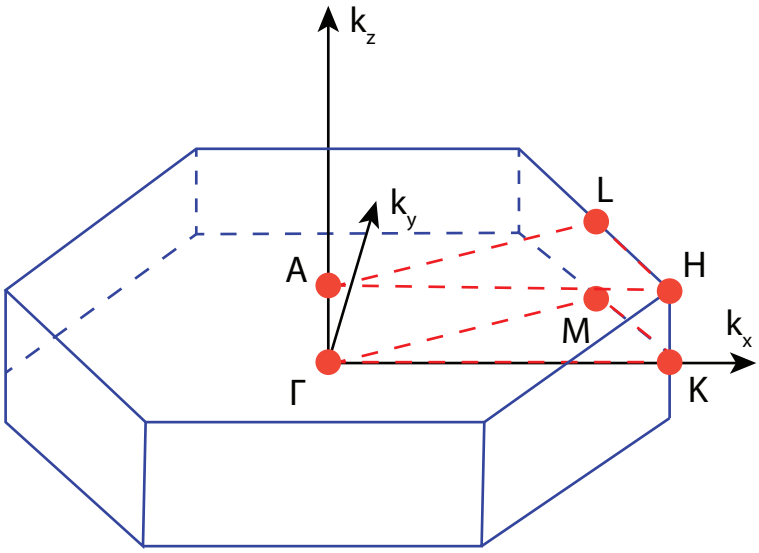

Figure 1.4: Unit cell of the reciprocal lattice or first Brillouin zone of an hexagonal crystal. The orange points marked with letters denote the high symmetry points. Taken from [49].

From equation (1.6) it can be deduced that, when having a two-dimensional system, the magnitude of the vector orthogonal to the plane tends to zero, due to that the value of the lattice constant c tends to infinity. For that, excitations are just represented in a plane in the first Brillouin zone, as can be seen in Figure 1.5. This plane includes the whole set of excitations for which the component of the wave vector $\mathbf{k}$ in the direction perpendicular to the plane are zero.

1.5.2 Synthesis

Zhang *et al.* [47] and Xu *et al.* [50] achieved to obtain blue phosphorene monolayers using the molecular beam epitaxy technique over a gold substrate on the crystallographic plane (111). They used black phosphorus as precursor. The sample was characterized using X ray photoelectron spectroscopy and STM. Some of the images obtained are shown in Figure 1.6. Following a similar methodology, it was also possible to obtain the same blue phosphorene monolayer over gold substrate (111) functionalized with

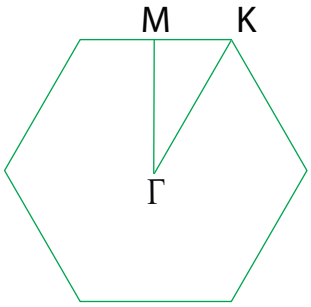

Figure 1.5: First Brillouin zone for a 2D material with an hexagonal structure as the blue phosphorene. The high-symmetry points are denoted with letters. The small triangle represents the irreducible Brillouin zone [49].

tellurium[51].

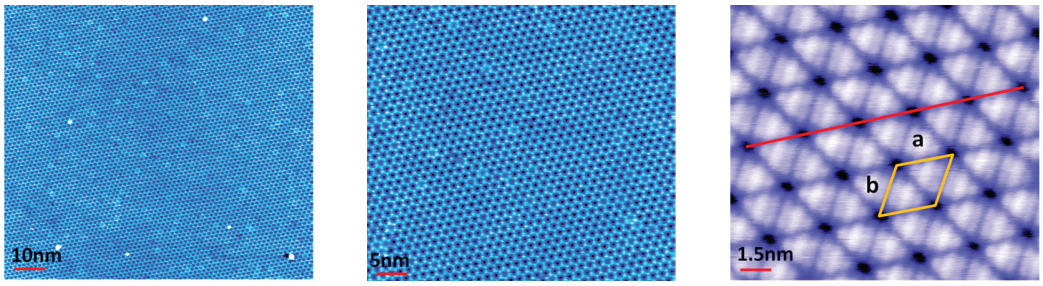

(a) (b) (c)

Figure 1.6: Images obtained with the STM of the blue phosphorene monolayer reported by Zhang *et al.* [47]. Panel (a) shows a large scale STM image of the single layer on Au(111) (V_{tip} = 0.9 V, 100 × 100 nm^2). Panel (b) shows a close-up STM image (V_{tip} = 0.9 V, 50 × 50 nm^2). Panel (c) shows a high resolution STM image (V_{tip} = 1.0 V, 8 × 8 nm^2). The unit cell of blue phosphorene is also highlighted.

1.5.3 Applications

Many works have been presented related to the change in the structure of blue phosphorene varying the number of stacked monolayers or varying the angle of one of those monolayers with respect to the others [46]. Some of the results are that the absorption of the bilayer structure is modified in the sense that

visible light could be absorbed, as a photovoltaic cell or a photodiode does. Also, in heterostructures composed of blue phosphorene and transition metal dichalchogenides the conversion efficiency of visible light is increased with respect to the pure blue phosphorene structure [52]. There is also a proposal of blue phosphorene and magnesium hydroxide as a photocatalyst to separate water molecules [53]. In the electronic devices area, blue phosphorene was proposed as a possible high mobility 2D material when mixed with fluoride [54], having Dirac cones in the band structure. Also, it could be used as a gate in a two dimensional field effect transistors [55], as a photodetector [56], working as Schottky barriers, mixed with black phosphorene [57] or even as a atmospheric gases sensor [58]. In the area of rechargable lithium batteries, blue phosphorene could be used to fabricate anodes [59], making the charge capacity bigger compared to graphite, which is the material used in the industry nowadays to produce this kind of batteries. Finally, an interesting property that could be useful in engineering electronic devices and thermal expansion materials, is that the thermic coefficient in this material in the temperature range of 0 to 350 K is negative, just as in graphene [60].

1.6 Scope of the thesis

In this project, a study of the electronic properties and linear optical response of blue phophorene will be performed. It is expected to obtain the band structure calculations and the linear optical susceptibilities spectra or dielectric function, using first principles methods. Approximations that do and do not consider the effects of many-body interactions are employed. Considering the effects of many-body interactions in the calculations would lead to a prediction of below-band-gap absorption, that could not been explained without that consideration.

1.6.1 Goals

- To perform a study of the linear optical properties of blue phosphorene that includes many-body interactions effects.
- To generate knowledge to the field of study of optical properties of 2D materials.

1.6.2 Objectives

- To do an exhaustive revision of the state of art of the optical response studies of blue phosphorene, that include the many-body interaction and excitonic effects.
- To perform first principles calculations, based on DFT, to optimize energetically the blue phosphorene crystalline structure.
- To calculate the band structure of blue phosphorene, within the DFT formalism, and including the energy corrections trough the GW approximation methodology.
- To obtain the linear optical response of blue phosphorene using the DFT and the Bethe-Salpeter equation formalism.
- To compare and analyse the general results of the study with those that have been already published, with an emphasis on the effects of the many-body interactions.

Chapter 2

Theoretical framework

In this chapter, some theoretical aspects, necessary to comprehend the methodology and the physics of the calculations, are developed. The fundamental mathematical expressions for the physical description of the phenomena are presented.

2.1 Atomic-system hamiltonian

The quantum mechanical, time-independent, description of a system composed of nuclei and electrons that interact with each other can be represented, in the non relativistic limit, by the hamiltonian

$$H = T_e + T_I + V_{ee} + V_{II} + V_{eI}, \tag{2.1}$$

where T_e (T_I) is the electrons (ions) kinetic energy, V_{ee} is the interaction potential among electrons, V_{II} is the interaction potential among ions and V_{eI} is the potential due to electron-ion interaction [61].

In general, equation (2.1) has to consider many-body effects, making it difficult to solve. One of the first approximations that can be done is that of considering the ions kinetic energy term as very close to zero, because the kinetic energy term goes as $1/M$, being M the mass of the nuclei. Due to the considerable difference between electron and nuclei mass, in a given external perturbation, the electrons will react almost instantaneously, considering their low inertia compared to the nuclei. This is the well-known Born-Oppenheimer approximation.

On the other hand, the interaction potential of the nuclei with one another contribute to the total energy but is not necessary to describe the electrons dynamical behavior so one can get rid of this term too. Now, the hamiltonian of the system can be written as

$$H = T_e + V_{ee} + V_{eI}. \tag{2.2}$$

To see the complexity of this formulation one has to explicitly write the terms in equation (2.2)

$$H(\mathbf{r}_1, \cdots, \mathbf{r}_N) = -\frac{\hbar}{2m_e}\sum_{i=1}^{N}\nabla_i^2 + \frac{1}{2}\sum_{i\neq j}\frac{\mathrm{e}^2}{|\mathbf{r}_i - \mathbf{r}_j|} + \sum_{i=1}^{N} V_{\text{ext}}(\mathbf{r}_i), \tag{2.3}$$

where $\hbar$ is Planck's constant, m_e the electron mass, e the electron charge and V_{ext} is equal to V_{eI}, the potential acting on the electron due to the nuclei. In (2.3), $\mathbf{r}_i$ represents electrons coordinates, and the sum runs over the total electrons in the system N.

2.2 The Kohn-Sham equations

2.2.1 Theoretical description

The fundamental tenet of density functional theory is that any property of a system of many interacting particles can be viewed as a functional of the ground state density $n_0(\mathbf{r})$; that is, one scalar function of position $n_0(\mathbf{r})$, in principle, determines all the information in the many-body wavefunctions for the ground state and all excited states. The attraction of density functional theory is evident by the fact that one equation for the density is remarkably simpler than the full many-body Schrodinger equation that involves $3N$ degrees of freedom for N electrons [61].

As was seen before, the Kohn-Sham approach replaces the original many-body problem using an independent-particle approximation. First, one "predict" the ground-state density of the many-body interacting system. This density can be used on an independent system with no interaction present. Then, using this new description, one can have a set of independent-particle equations that can be solved by numerical means. The resulting density can then be extrapolated to the original many-body system, so one can have an

actual answer for the problem of determining the properties of that system. As mentioned by the authors of the method in 1965 [25], it is necessary to include the effects of the many-body interactions using the exchange-correlation functional that has to be accurate in order to give good results.

The variational principle relates the energy of the system with the density in a functional equation. The total energy $E[n(\mathbf{r})]$ is composed of different terms, since

$$E[n(\mathbf{r})] = T_s[n(\mathbf{r})] + E_{XC}[n(\mathbf{r})] + E_H[n(\mathbf{r})] + V_{ext}[n(\mathbf{r})], \tag{2.4}$$

where $T_s[n(\mathbf{r})]$ is the kinetic energy of a system of non-interacting electrons with density $n(r)$, $E_{XC}[n(\mathbf{r})]$ is the exchange and correlation energy functional of a interacting system with density $n(r)$, $E_H[n(\mathbf{r})]$ is the Hartree energy term and $V_{ext}[n(\mathbf{r})]$ is the potential energy term. In order to describe the independent-particle equations in the Kohn-Sham approach one has to construct the hamiltonian of the system using potentials, which are related to the energy terms by a functional derivative with respect to the density in each case. The hamiltonian in the Kohn-Sham approach is

$$H_{\mathrm{KS}} = T_e + V_{\mathrm{H}} + V_{\mathrm{XC}} + V_{\mathrm{ext}}, \tag{2.5}$$

where V_{H} is Hartree's potential and V_{XC} is the exchange-correlation potential. The many-body kinetic energy (a functional of the density also, as pointed out by Hohenberg and Kohn) contribution is contained in the exchange-correlation energy (potential) term, so the term T_e is referred to the independent-particle kinetic energy.

Knowing the terms explicitly for the hamiltonian, it is possible to obtain the wavefunction of the different states $\phi_i(\mathbf{r}_i)$ from the set of equations

$$H_{\mathrm{KS}}\phi_i = \varepsilon_i\phi_i, \tag{2.6}$$

where ε_i is the Kohn-Sham eigenvalue of the energy for the i-th state.

These equations have to be solved self-consistently: the wavefunctions obtained by solving the equations are used to calculate the density, which has to be the same as the one that was used for constructing the potential in the hamiltonian of the system. Following this algorithm, for calculating the ground-state density, one only has to find the density that minimizes the energy functional (second HK theorem). In Figure 2.1 a flow chart is shown

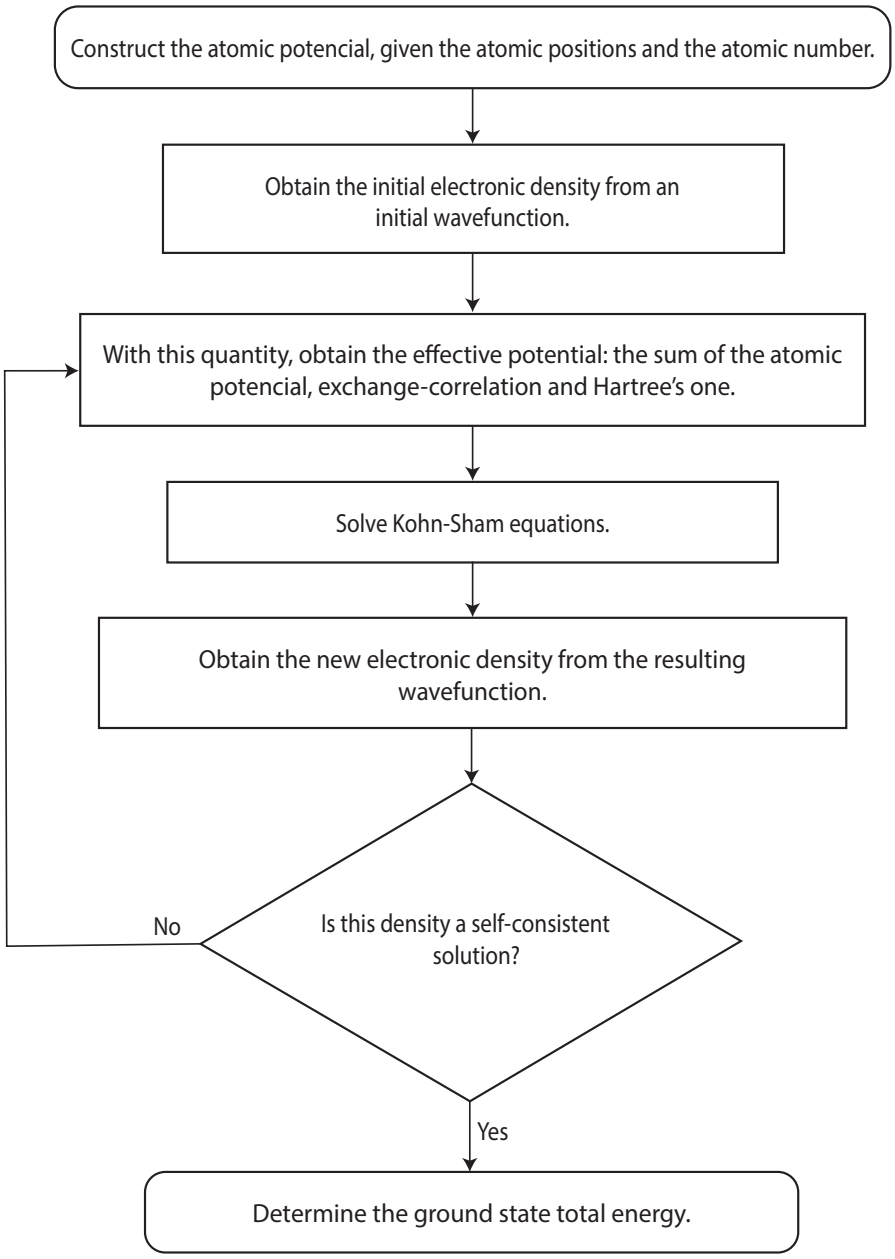

Figure 2.1: Flow chart describing the procedure for reaching self-consistency for ground-state density and energy calculations within the Kohn-Sham approach [49].

with the procedure necessary in order to obtain the ground-state energy of the system in this approach.

Firstly, the ionic potential is built from the atomic positions in the system. Then, an initial density is obtained, given an initial wavefunction that is used for constructing the effective potential. Next, the Kohn-Sham equations can be solved, from where a new wavefunction will be obtained as a solution and, consequently, a new density. At this point one has to answer the question: is this a self-consistent solution? If the answer is yes, then the density can be used to generate the same effective potential constructed at the beginning of the calculation. If the answer is no, the process is repeated until self-consistency is reached: a new effective potential is built with the aid of the new calculated density and the Kohn-Sham equations are once again formed to be solved. Finally one can proceed to calculate the total energy of the system, that is, the ground-state energy.

2.2.2 Modern first principles calculations

Two difficulties must be overcome to reach a solution in DFT calculations that use the Kohn-Sham approach: a wave function must be calculated for each of the infinite number of electrons in the system, and, since each electronic wave function extends over the entire solid, the basis set required to expand each wave function is infinite. Both problems can be surmounted by performing calculations on periodic systems and applying Bloch's theorem to the electronic wavefunctions [62]. As was mentioned, one can describe these wavefunctions as a product of a periodic function $f_i(\mathbf{r})$, with lattice periodicity and a plane wave

$$\phi_i(\mathbf{r}) = \mathrm{e}^{i\mathbf{k}\cdot\mathbf{r}} f_i(\mathbf{r}), \tag{2.7}$$

where $\mathbf{k}$ is a wave vector. This periodic function $f_i(\mathbf{r})$ can be expanded using a discrete set of plane waves using the reciprocal lattice vectors $\mathbf{G}$ as basis wave vectors as

$$f_i(\mathbf{r}) = \sum_{\mathbf{G}} c_{i,\mathbf{G}} \mathrm{e}^{i\mathbf{G}\cdot\mathbf{r}}. \tag{2.8}$$

Reciprocal lattice vectors are defined as $\mathbf{G}\cdot\mathbf{R} = 2\pi m$, being $\mathbf{R}$ a lattice vector and m an integer number. Then, using equations (2.7) and (2.8), the wavefunctions can be written as

$$\phi_i(\mathbf{r}) = \sum_{\mathbf{G}} c_{i,\mathbf{k}+\mathbf{G}} \mathrm{e}^{i(\mathbf{k}+\mathbf{G})\cdot\mathbf{r}}, \tag{2.9}$$

which means that every electronic wavefunction can be written as a sum of plane waves with wave vectors equals to $(\mathbf{k}+\mathbf{G})$. So, using the plane wave expansion for the electronic wavefunctions (equation (2.9)), the Kohn-Sham equations take the form [62]

$$\sum_{\mathbf{G}'}\left[\frac{\hbar^2}{2m}|\mathbf{k}+\mathbf{G}|^2\delta_{\mathbf{G}\mathbf{G}'}+V_{ext}(\mathbf{G}-\mathbf{G}')+V_H(\mathbf{G}-\mathbf{G}')+V_{XC}(\mathbf{G}-\mathbf{G}')\right]c_{i,\mathbf{k}+\mathbf{G}'}=\varepsilon_i c_{i,\mathbf{k}+\mathbf{G}}, \tag{2.10}$$

where the potentials are given by their Fourier transforms. In order to solve the set of equations one has to define two quantities: the number of $\mathbf{k}$ points and the cut-off energy for the plane waves basis set

$$E_{\text{cut}-\text{off}}=\frac{\hbar^2}{2m}|\mathbf{k}+\mathbf{G}|^2. \tag{2.11}$$

Bloch's theorem changes the problem of calculating an infinite number of electronic wave functions to one of calculating a finite number of electronic wave functions at an infinite number of $\mathbf{k}$ points. The occupied states at each $\mathbf{k}$ point contribute to the electronic potential in the bulk solid so that, in principle, an infinite number of calculations are needed to compute this potential. However, the electronic wave functions at $\mathbf{k}$ points that are very close together will be almost identical. Hence it is possible to represent the electronic wave functions over a region of $\mathbf{k}$ space by the wave functions at a single $\mathbf{k}$ point. In this case the electronic states at only a finite number of $\mathbf{k}$ points are required to calculate the electronic potential and hence determine the total energy of the solid. The magnitude of any error in the total energy due to inadequacy of the $\mathbf{k}$-point sampling can always be reduced by using a denser set of $\mathbf{k}$ points. The computed total energy will converge as the density of $\mathbf{k}$ points increases, and the error due to the $\mathbf{k}$-point sampling then approaches zero.

Also, Bloch's theorem states that the electronic wave functions at each $\mathbf{k}$ point can be expanded in terms of a discrete plane wave basis set. In principle, an infinite plane wave basis set is required to expand the electronic wave functions. However, the coefficients $c_{i,\mathbf{k}+\mathbf{G}}$ for the plane waves with small

kinetic energy are usually more important than those with large kinetic energy. Thus the plane wave basis set can be truncated to include only plane waves that have kinetic energies values lower than some particular cut-off energy. Introduction of an energy cut-off to the discrete plane-wave basis set produces a finite basis set. The truncation of the plane wave basis set at a finite cut-off energy will lead to an error in the computed total energy. However, it is possible to reduce the magnitude of the error by increasing the value of the cut-off energy until the calculated total energy converges.

2.3 Approximating the exchange-correlation functional for DFT calculations

The key problem of electronic structure is that electrons form an interacting many-body system. From this, the correlation and exchange energy terms are crucial in defining a theory for the description of the electrons in matter in the independent-particle approach.

The role of correlation among electrons stands out as defining the great questions and challenges of the field of electronic structure today; the difference between the many-body energy of an electronic system and the energy of the system calculated in the Hartree-Fock approximation is called the correlation energy [62]. In the case of the exchange energy, one can think the problem by considering electrons with two possible spin states. The charge distribution depends on whether the spins are parallel or antiparallel since the Pauli exclusion principle excludes two electrons of the same spin from being at the same place at the same time. Thus the electrostatic energy of a system will depend on the relative orientation of the spins: the difference in energy defines the exchange energy [63]. If the spin were not present, the problem will remain since, as obtained by Dirac, the exchange term is the contribution to the energy arising from the antisymmetry of the wavefunction under permutation of electrons, indistinguishable between them [64]. This exchange energy can be large in comparison with others energetic contributions to the electronic description, so, in including this term, the theory should arrive to more precise results.

The exchange-correlation functional $E_{\mathrm{XC}}[n]$, as was mentioned before, is vital in Kohn-Sham approximation. Even though this functional can be very

complex, it has been possible to approximate it in a simple manner [61]. The two principal approximations used in the theory are presented here.

2.3.1 Local Density Approximation

Kohn and Sham, in their original work [25], pointed out that solids can often be considered as close to the limit of the homogeneous electron gas. In that limit, the exchange and correlation are local in character, and they proposed making a Local Density Approximation (LDA) of this energy functional, in which the exchange-correlation energy density at each point is assumed to be the same as in a homogeneous electron gas with that density, that is

$$E_{XC}[n(\mathbf{r})] = \int n(\mathbf{r})\epsilon_{xc}(n(\mathbf{r}))\,\mathrm{d}r^3. \tag{2.12}$$

The only information needed is the exchange correlation energy as a function of the density ($\epsilon_{xc}(n(\mathbf{r}))$) for the system.

The rationale for the LDA is that for typical densities found in solids, the range of the effects of exchange and correlation is rather short [61]. It is also important to say that this approximation can be extended, considering in the description the spin-dependent electron density, giving place to what is known as the Local Spin Density Approximation or LSDA.

2.3.2 Generalized Gradient Approximation

The actual success of the LDA has led to the development of the Generalized Gradient Approximation or GGA with marked improvement over many cases. This approximation had made possible the development of DFT calculations in chemistry due to its great accuracy: there are more rapidly varying density regions in atoms than in molecules or solids.

The key idea is to use a functional of the magnitude of the gradient of the density ($|\nabla n|$) with the position as well as the value of n at each point. The exchange-correlation functional in a generalized form can be written as

$$E_{XC}[n(\mathbf{r})] = \int n(\mathbf{r})\epsilon_{xc}(n(\mathbf{r}), |\nabla n|, ...)\,\mathrm{d}r^3, \tag{2.13}$$

where the points denote that the exchange correlation energy could have a dependency on higher order terms on the gradient of the density.

Another advantage of this approximation is that the resulting binding energy is corrected with respect to the LDA, which has an overbinding in some cases, thus improving the agreement with experiment.

2.4 Pseudopotentials

Conduction electron wavefunctions are usually smoothly varying in the region between the ion cores, but have a complicated nodal structure in the region close to the cores. Outside the core the potential energy that acts on the conduction electrons is relatively weak: it is only the Coulomb potential of the charged ion core and is reduced markedly by the electrostatic screening of other conduction electrons. In this outer region the conduction electron wavefunctions are smoothly varying. This argument leads naturally to the idea that we might replace the actual potential energy (and filled shells) within core region by an effective potential energy that gives the same wavefunctions outside the core as are given by the actual ion cores [63].

A pseudopotential, in electronic structure calculations, is that ionic effective potential that replaces the strong Coulomb potential of the nuclei and acts on the valence electrons of the atom. The use of pseudopotentials is a convenient tool to perform electronic structure calculations, since in an all-electron calculation, an extremely large plane wave basis set, and a vast amount of computational time would be required to calculate the electronic wave functions.

The pseudopotential can be generated in an atomic calculation and then be used to determine properties of the valence electrons in molecules or solids. Even more, considering that the pseudopotential for a problem is not unique nor exact, the user, given the case, can choose which one can be more useful for his own calculation [61].

2.5 The dielectric function

The dielectric and conductivity functions are the most important response functions in condensed matter physics because they determine the optical properties of materials, and its electrical conductivity [61].

The dielectric function $\epsilon(\omega)$ or electric permittivity of a material describes

its response to an external perturbation due to an electromagnetic field. It depends sensitively on the electronic band structure of the crystal and has a dependency on the frequency ω of the incident field. This quantity has a complex nature and generally is written as

$$\epsilon(\omega) = \epsilon_1(\omega) + i\epsilon_2(\omega), \tag{2.14}$$

where $\epsilon_1(\omega)$ and $\epsilon_2(\omega)$ are the real and imaginary parts, respectively, and are related by the Kramers-Kronig relations [64]. This quantity is not directly accessible experimentally from optical measurement but it has a direct relation with the complex index of refraction (which is an accessible function), given by [63]

$$\hat{n}(\omega) = \sqrt{\epsilon(\omega)\mu(\omega)}, \tag{2.15}$$

where $\mu(\omega)$ is the magnetic permittivity of the medium. For a non magnetic material, $\mu(\omega)$ can be considered as unity so the last expression can be written as

$$\hat{n}(\omega) = \sqrt{\epsilon(\omega)}. \tag{2.16}$$

In its components, the complex refractive index is expressed as

$$\hat{n}(\omega) = n_0(\omega) + i\kappa(\omega), \tag{2.17}$$

where $n_0(\omega)$ is the ordinary refractive index, defined as the quotient between the speed of light in vacuum and the speed of the light in the medium of analysis, and $\kappa(\omega)$ is the extinction coefficient, that is directly related to the absorption of the incident light. Using equations (2.14), (2.16) and (2.17), the relation between both the complex electric permittivity, and the complex refractive index can be given for its constitutive parts

$$n_0(\omega) = \sqrt{\frac{|\epsilon(\omega)| + \epsilon_1(\omega)}{2}}, \tag{2.18}$$

$$\kappa(\omega) = \sqrt{\frac{|\epsilon(\omega)| - \epsilon_1(\omega)}{2}}. \tag{2.19}$$

Classically, material's polarization varies linearly with the applied electric field as

$$\mathbf{P}(\omega) = \epsilon_0\chi(\omega)\mathbf{E}(\omega), \tag{2.20}$$

where $\mathbf{P}(\omega)$ is the polarization, ϵ_0 the dielectric permittivity of vacuum, $\chi(\omega)$ the electric linear susceptibility of the material and $\mathbf{E}(\omega)$ is the electric field oscillating at frequency ω. The dielectric function is directly related to the electric susceptibility as

$$\chi(\omega) = \epsilon(\omega) - 1. \tag{2.21}$$

In terms of the real and imaginary parts of both quantities, the relations are of the form

$$\epsilon_1(\omega) = 1 + \mathrm{Re}\,\chi(\omega), \tag{2.22}$$
$$\epsilon_2(\omega) = \mathrm{Im}\,\chi(\omega). \tag{2.23}$$

The linear susceptibility is a tensor so, in terms of its Cartesian components, equation (2.20) can be rewritten as

$$P_i(\omega) = \epsilon_0 \chi_{ij}(\omega) E_j(\omega). \tag{2.24}$$

In general, χ_{ij} is written as χ, referring to one of its components. Polarization equation (2.24) indicates that the response of a medium to an oscillatory field in time at a given frequency ω and polarized in j direction, is the electric polarization of the medium in the direction i and that oscillates at the same frequency ω.

Quantum mechanically, the problem of dispersion of light by dielectric media can be thought of that of determining the net effect on the wavefunctions of the electrons in defined states when an external perturbation is applied i.e. an external electric field that varies with time [65]. The imaginary part of the susceptibility, that can be obtained with Fermi's golden rule, gives a better physical idea of the absorption of light. This response arises from the coupling, caused by the electric field, of occupied states with unoccupied states; the absorption can only occur if the two states differ in energy by $\hbar\omega$ and the transitions must be between states that have the same wave vector $\mathbf{k}$ [64].

Within first principle calculations, the expression for obtaining linear susceptibility is somewhat different, although the considerations for obtaining are almost the same, due to the proper quantum character of the formalism. In the independent-particle approximation, discussed earlier, the expression is

$$\chi_{ij}(-\omega, \omega) = \frac{1}{\Omega} \sum_{nm\mathbf{k}} f_{nm}(\mathbf{k}) \frac{r^i_{nm}(\mathbf{k}) r^j_{mn}(\mathbf{k})}{\omega_{mn}(\mathbf{k}) - \omega}, \tag{2.25}$$

where Ω is the unit cell volume, $\mathbf{r}_{mn}$ are the matrix elements of the position operator, $\mathbf{k}$ is the wave vector, ω_{mn} are the transition frequencies of the electrons ($\omega_{mn} = \omega_m - \omega_n$), where the subindexes m y n represent conduction and valence states, respectively; considering also that $f_{nm} = f_n - f_m$, being f_n Fermi's factor (define as f_n is equal to one if n is a valence state and f_n is equal to zero if n is a conduction state). This sum runs over all the valence and conduction states and the total number of wave vectors $\mathbf{k}$ in reciprocal space [66].

2.6 The GW approximation

The actual challenge for electronic structure theory is to provide universal methods that accurately describe real systems in nature.

Despite the impressive agreement of many DFT calculations for ground state properties [67], the same calculations often lead to disastrous predictions for excitations [68]. The fundamental energy band gap is the key issue, widely used approximate functionals in DFT lead to band gap values that are significantly lower than experimental values for essentially all materials. These low band gaps are not intrinsic to the Kohn-Sham approach and are greatly improved by better treatment of the non-local exchange [61].

In 1965 L. Hedin published his famous work related to the calculation of the one-particle Green's function, which gives information of the low-excitation spectra [69]. The main results are pointed out and listed by the author at the end of the paper as:

"(1) A set of self-consistent equations for the one electron Green's function involving a screened potential."

These set of self-consistent equations are derived in the paper and are now known as the Hedin's equations; they are presented and described in section 2.6.3 of this work.

"(2) A variational formulation for each self-consistent equation."

The mathematical formulation of every equation is presented in terms of specific functional operations.

"(3) A specific approximation for the first-order equation".

The referred approximation is the well known GW approximation, proposed by him as a way of representing the self-energy operator up to first order. This results when the Vertex function is approximated to zeroth-order, in terms of the screened Coulomb potential, making the self-consistent set of equations easier to solve. This is described mathematically at the end of section 2.6.3 of this work.

It is important to mention that this approach is relevant since it gives a better description of some materials properties compared with that of the Kohn-Sham approach, though with the necessity of a greater computational effort to perform the actual calculations.

In the following subsections, the quasiparticle definition is presented first. Then, the Green's functions and the self-energy operator are described. After that, the set of self-consistent equations proposed by Hedin are presented; the GW approximation is then introduced. Finally, some details about the algorithms used to calculate the self-energy operator and the GW corrections are given.

2.6.1 Quasiparticles

A successful approximation for the determination of excited states is based on the quasiparticle concept. The Coulomb repulsion between electrons leads to a depletion of negative charge around a given electron and the ensemble of this electron and its surrounding positive screening charge forms a quasiparticle [70] (see Figure 2.2). One could also think in quasiparticles as collective excitations present at low energies in the materials [71].

In a solid, a real electron, or bare particle, repels the other electrons via the Coulomb potential and surrounds itself with a positively charged polarization cloud. The positive screening charge and the bare electron form a quasiparticle which weakly interacts with other quasiparticles via a screened rather than the bare Coulomb potential. The quasiparticle lifetime is finite since quasiparticles are only approximate eigenstates of the N-electron Hamiltonian. The residual interaction between the quasiparticles leads to a complex energy whose imaginary part is inversely proportional to the quasiparticle life time.

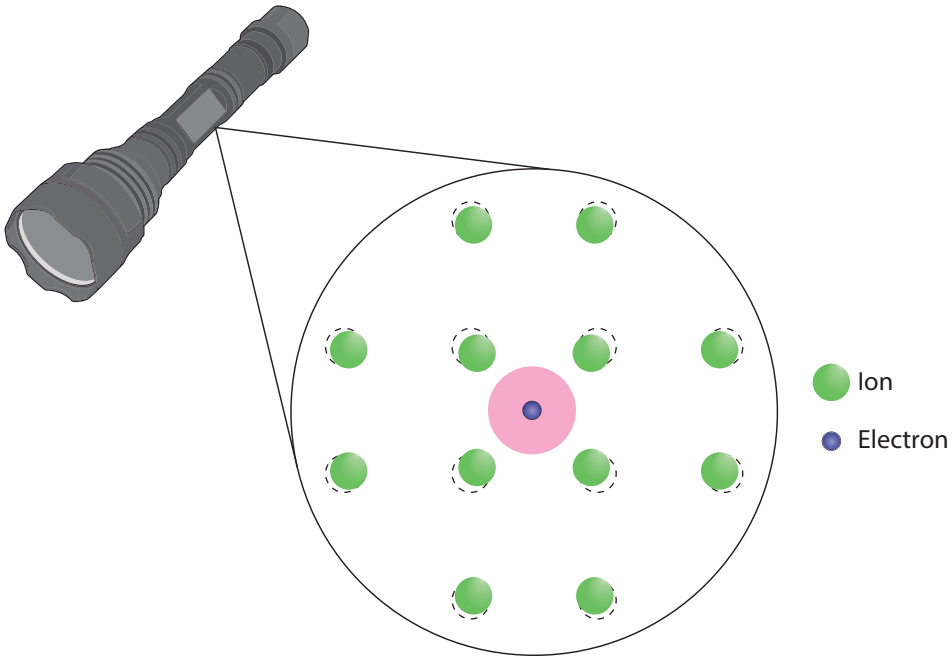

Figure 2.2: Pictorical description of a quasiparticle in a solid. An electron in a solid interacts with the crystal lattice in such a way that the bare particle is now surrounded by a cloud of positive charge, represented here with the pink circle in which the elctron is enclosed. The attraction between the electron and the ions, due to the electric force, tends to move the ions, towards the electron, from its equilibrium position (the dashed-line circles). The net movement of the ions has been exagerated for an easier comprehension.

2.6.2 Propagators and the self-energy operator

The mathematical description of quasiparticles is based on the single-particle Green function G, whose exact determination requires complete knowledge of the quasiparticle self-energy Σ. The self-energy is a non-Hermitian, energy-dependent, and non-local operator that describes exchange and correlation effects beyond the Hartree approximation. A determination of the self-energy can only be approximate, and a working scheme for the quantitative calculation of excitation energies in metals, semiconductors, and insulators is the so-called dynamically screened interaction or the GW approximation (GWA). In this approximation, the self-energy Σ is expanded linearly in terms of the screened interaction W, $\Sigma \approx GW$. An exact determination of the self-energy

for real systems is not possible, since it contains all the complexities of the many-body system [70].

The equation that rules the behavior of quasiparticles is, neglecting spin degrees of freedom [72],

$$\left[-\frac{1}{2}\nabla^2 + V_H + V_{ext}\right]\Psi_i(\mathbf{r}) + \int \Sigma(\mathbf{r},\mathbf{r}';E_i)\Psi_i(\mathbf{r}')\mathrm{d}\mathbf{r}' = E_i\Psi_i(\mathbf{r}), \tag{2.26}$$

being E_i and Ψ_i the quasiparticle energy and wavefunction, respectively.

Quasiparticle properties such as energies, life times, and expectation values of single-particle operators such as the density and the total energy of a many-body system are determined by the single-particle Green function G or single-particle propagator [73]

$$G(\mathbf{r}t,\mathbf{r}'t') = -i\left\langle N,0\right| T[\hat{\Psi}(\mathbf{r}t)\hat{\Psi}^\dagger(\mathbf{r}'t')]\left|N,0\right\rangle, \tag{2.27}$$

with $|N,0\rangle$ is the ground state of the N-electron Hamiltonian, $\hat{\Psi}(\mathbf{r}t) = \exp\left(i\hat{H}t\right)\hat{\Psi}(\mathbf{r})\exp\left(-i\hat{H}t\right)$ is the fermion annihilation operator in the Heisenberg representation, $\hat{\Psi}^\dagger(\mathbf{r}t)$ is the corresponding creation operator, and T is the time-ordering operator [1]. For $t > t'(t < t')$ G describes the propagation of a particle (hole) added to the many-body system described by $\hat{H}$, i.e., G describes the dynamics of the $N \to N \pm 1$ excitations in an N-electron system. Note that G is a function of only six spatial degrees of freedom and hence much more manageable than the N-electron wavefunction with $3N$ degrees of freedom [73]. The physical interpretation of the Green function is that for $t > t'$ it gives the probability amplitude that a particle added at $\mathbf{r}'t'$ will propagate to $\mathbf{r}t$; and for $t > t'$ it gives the probability amplitude that a hole created at $\mathbf{r}t$ will propagate to $\mathbf{r}'t'$. From the Green function, one can obtain the following [73, 75]:

[1] For two operators $A(x)$ and $B(y)$ that depend on spacetime coordinates x and y, on a fermion system, the time ordering operator is defined as

$$T[A(x)B(y)] := \begin{cases} A(x)B(y) & \text{if } \tau_x > \tau_y, \\ -B(y)A(x) & \text{if } \tau_x < \tau_y, \end{cases}$$

where τ_x and τ_y denote scalar time-coordinates of the points x and y [74].

a) the expectation value of any single-particle operator in the ground state,

b) the ground-state energy,

c) and the one-electron excitation spectrum.

Considering a complete set of eigenstates, the quasiparticles energies E_i can be given by the poles of the Green function [72]

$$G(\mathbf{r},\mathbf{r}';E)=\sum_i \frac{\Psi_i(\mathbf{r})\Psi_i^*(\mathbf{r}')}{E-E_i}. \tag{2.28}$$

The excitation energies of the N-electron system can be written as

$$E_j=\begin{cases} E_j^{N+1}-E_0^N & \text{if } E_j>\mu, \\ E_0^N-E_j^{N-1} & \text{if } E_j<\mu, \end{cases} \tag{2.29}$$

where E_0^N is the ground-state energy of the electron system of N electrons, j labels the excited states and μ is the chemical potential [2] And the excitation wavefunctions as

$$\Psi_j(\mathbf{r})=\begin{cases} \langle N,0|\,\hat{\psi}(\mathbf{r})\,|N+1,j\rangle & \text{if } E_j>\mu, \\ \langle N-1,j|\,\hat{\psi}(\mathbf{r})\,|N,0\rangle & \text{if } E_j<\mu. \end{cases} \tag{2.30}$$

The non-interacting single-particle Green function $G_0(\mathbf{r},\mathbf{r}';E)$ describes the propagation of a particle in a system of $N+1$ non-interacting particles for the case where exchange and correlation effects are neglected

$$G_0(\mathbf{r},\mathbf{r}';E)=\sum_i \frac{\phi_i(\mathbf{r})\phi_i^*(\mathbf{r}')}{E-\epsilon_i}, \tag{2.31}$$

where $\phi_i(\mathbf{r})$ are the complete set of orthonormalized single-particle wave functions and ϵ_i the real, independent-particle energies.

[2] The chemical potential of a particle system is defined as the ratio of the change of free energy and the change of the particle number. In intrinsic semiconductors, and in the grand canonical ensemble, the chemical potential $\mu(N+1)$ for the $N+1$ particle system tends to the following values: when $T\to 0$, $\mu(N+1)$ tends to the bottom of the conduction band; wheareas for $N\to\infty$, $\mu(N+1)$ tends to the middle of the gap [76].

The time development of the interacting Green function is determined by Dyson's equation

$$\begin{aligned} G(\mathbf{r},\mathbf{r}';E) =& G_0(\mathbf{r},\mathbf{r}';E) \\ &+ \int\int G_0(\mathbf{r},\mathbf{r_1};E)\Sigma(\mathbf{r_1},\mathbf{r_2};E)G(\mathbf{r_2},\mathbf{r}';E)\mathrm{d}\mathbf{r_1}\mathrm{d}\mathbf{r_2}, \end{aligned} \tag{2.32}$$

which can be written as [73]

$$G^{-1} = (G_0)^{-1} - \Sigma. \tag{2.33}$$

Instead of determining the quasiparticle energies indirectly as poles of the Green function, note that it is more convenient to obtain the quasiparticles energies from the quasiparticle equation (2.26).

2.6.3 The Hedin's equations

The exact self-energy can be obtained from the set of integro-differential equations known as the Hedin's equations [69, 70], which are written as[3]

$$\Sigma(1,2) = i\int G(1,4)W(1^+,3)\Gamma(4,2;3)\mathrm{d}(3,4) \tag{2.34}$$

$$W(1,2) = v(1,2) + \int W(1,3)P(3,4)v(4,2)\mathrm{d}(3,4) \tag{2.35}$$

$$P(1,2) = -i\int G(2,3)G(4,2)\Gamma(3,4;1)\mathrm{d}(3,4) \tag{2.36}$$

$$\begin{aligned} \Gamma(1,2;3) =& \delta(1,2)\delta(1,3) \\ &+ \int \frac{\delta\Sigma(1,2)}{\delta G(4,5)} G(4,6)G(7,5)\Gamma(6,7;3)\mathrm{d}(4,5,6,7), \end{aligned} \tag{2.37}$$

where 1, 2, etc., indicates a short notation for combined space and time coordinates, $1^+ = (\mathbf{r_1}t_1 + \eta)$, with $\eta > 0$ and infinitesimal, and $v(1,2)$ represents

[3] Cf. Appendix A to see the notation used to express the functional derivatives throughout the text.

the bare Coulomb interaction (the Coulomb potential that decays as $1/r$). The screened Coulomb interaction W includes the effects of the screening of the medium in the interaction between particles, which reduce the total electric field felt by a charge. The vertex function Γ is given by the variation of the inverse Green function with respect to a change in the total potential or, alternatively, by the variation of the self-energy with respect to δV

$$\Gamma(1,2;3) = -\frac{\delta G^{-1}(1,2)}{\delta V(3)} = \delta(1,2)\delta(1,3) + \frac{\delta\Sigma(1,2)}{\delta V(3)}. \tag{2.38}$$

Considering the application of a small perturbation δV_{ext} to the many body system, the irreducible polarizability P is defined as the change in the density upon a change in the total potential $\delta V = \delta V_H + \delta V_{ext}$,

$$P(1,2) = \frac{\delta n(1)}{\delta V(2)}. \tag{2.39}$$

From these equations, quasiparticle self-energy can be determined iteratively, beginning from the determination of the vertex function [70].

The simplest approximation sets the vertex function to unity, and then the self-energy as the product of the self-consistent single-particle propagator G and the self-consistent dynamically screened interaction potential W. This is called the GW approximation. The corresponding expressions thus are [69]

$$\Sigma(1,2) = iG(1,2)W(1^+,2) \tag{2.40}$$

$$W(1,2) = v(1,2) + \int W(1,3)P(3,4)v(4,2)\mathrm{d}(3,4) \tag{2.41}$$

$$P(1,2) = -iG(1,2)G(2,1). \tag{2.42}$$

In principle, the GWA, for the self-energy, requires a self-consistent determination of the single-particle propagator G and the screened interaction potential W. All GWA calculations start from a suitably chosen one-particle Hamiltonian whose eigenfunctions and eigenvalues are used to construct the single-particle propagator G, the screened interaction W, and the self-energy Σ. The independent-particle Hamiltonian of choice is a DFT Hamiltonian.

Dinamic effects in the screening process are important since it introduces energy-dependet correlation effects. Phenomenologically, quasiparticles drag

their polarization cloud behind them. The screened interaction W can also be expressed in terms of the inverse dielectric matrix ϵ^{-1}. Rather than using the integral equation, W can be determined as a convolution of the inverse dielectric matrix with the bare Coulomb interaction potential in real space [70]

$$W(\mathbf{r},\mathbf{r}';\omega) = \int \epsilon^{-1}(\mathbf{r},\mathbf{r}'';\omega)v(\mathbf{r}'',\mathbf{r}')\mathrm{d}\mathbf{r}''. \tag{2.43}$$

This convolution can be transformed in reciprocal space as

$$W_{\mathbf{G},\mathbf{G}'}(\mathbf{q};\omega) = \frac{4\pi}{|\mathbf{q}+\mathbf{G}|^2}\epsilon^{-1}_{\mathbf{G},\mathbf{G}'}(\mathbf{q};\omega), \tag{2.44}$$

where $\mathbf{q}$ represents a vector in the reciprocal space. The irreducible polarizability P determines the dielectric matrix via

$$\epsilon(\mathbf{r},\mathbf{r}';\omega) = \delta(\mathbf{r}-\mathbf{r}') - \int v(\mathbf{r},\mathbf{r}'')P(\mathbf{r}'',\mathbf{r}';\omega)\mathrm{d}\mathbf{r}''. \tag{2.45}$$

It is important to note that to describe screening in solids in the random phase approximation (RPA), one uses equation (2.42). In the independent-particle approach, the interacting polarizability is replaced by the independent-particle polarizability P_0, where the propagators are now the single-particle non-interacting Green's function G_0, evaluated at the corresponding coordinates. Within the RPA, the dielectric matrix in reciprocal space can be written as

$$\epsilon_{\mathbf{G},\mathbf{G}'}(\mathbf{q};\omega) = \delta_{\mathbf{G},\mathbf{G}'} - \frac{4\pi}{|\mathbf{q}+\mathbf{G}|^2}P_{\mathbf{G},\mathbf{G}'}(\mathbf{q};\omega) \tag{2.46}$$

and, the polarizability P_0 is given as

$$\begin{aligned} P_{0;\mathbf{G},\mathbf{G}'}(\mathbf{q};\omega) = \frac{2}{V}\sum_{vc}^{\text{occ + unocc}}\sum_{\mathbf{q}}^{\text{BZ}}\sum_{\mathbf{G},\mathbf{G}'} \\ M^{cv}_{\mathbf{G}}(\mathbf{k},\mathbf{q})[M^{cv}_{\mathbf{G}'}(\mathbf{k},\mathbf{q})]^* \\ \times\left[\frac{1}{\omega+\epsilon_{c\mathbf{k}-\mathbf{q}}-\epsilon_{v\mathbf{k}}-i\eta} - \frac{1}{\omega-\epsilon_{c\mathbf{k}-\mathbf{q}}+\epsilon_{v\mathbf{k}}-i\eta}\right] \end{aligned} \tag{2.47}$$

where $M^{cv}_{\mathbf{G}}(\mathbf{k},\mathbf{q})$ represents a matrix element in reciprocal space defined as

$$M^{cv}_{\mathbf{G}}(\mathbf{k},\mathbf{q}) = \int \phi^*_{c\mathbf{k}-\mathbf{q}}(\mathbf{r})\mathrm{e}^{-i(\mathbf{q}+\mathbf{G})\cdot\mathbf{r}}\phi_{v\mathbf{k}-\mathbf{q}} = \sum_{\mathbf{G}'} t^*_{c\mathbf{k}-\mathbf{q}}(\mathbf{G}'-\mathbf{G})t_{v\mathbf{k}}(\mathbf{G}'), \tag{2.48}$$

c and v stand for a conduction or valence state, respectively, and we have use the definition of a Bloch state ϕ_i of equation (2.9), where $t_{m\mathbf{k}}$ represents the coefficients of the terms in the expansion. The last summation in equation (2.47), in principle, has to be calculated for an infinite set of reciprocal lattice vectors $\mathbf{G}$ but an energy cut-off can be defined in the same sense as in a Kohn-Sham calculation. The sum over the band indexes cv should extend up to infinity although in practice only a finite number of occupied and unoccupied states can be used. Also, for determining the frequency dependence of the dielectric response, one can approximate the dielectric matrix using plasmon-pole models and thus reducing the computational effort needed [70].

2.6.4 The calculation of the self-energy

In real calculations, the self-energy operator is splitted into two different parts to perform the complete calculation:

$$\Sigma = \Sigma^X + \Sigma^C(E). \tag{2.49}$$

These two parts are referred as the bare exchange contribution Σ^X and the energy dependent correlation contribution $\Sigma^C(E)$ and can be calculated independently [70].

The expression for the exchange part is

$$\langle m, \mathbf{k}| \Sigma^X |l, \mathbf{k}\rangle = -\frac{4\pi}{V} \sum_{v}^{\text{occ}} \sum_{\mathbf{q}}^{\text{BZ}} \sum_{\mathbf{G}} \frac{M^{vl}_{\mathbf{G}}(\mathbf{k}, \mathbf{q})[M^{vm}_{\mathbf{G}}(\mathbf{k}, \mathbf{q})]^*}{|\mathbf{q} + \mathbf{G}|^2}. \tag{2.50}$$

The last summation in equation (2.50), in principle, has to be calculated for an infinite set of reciprocal lattice vectors $\mathbf{G}$ but an energy cut-off can be defined in the same sense as in a Kohn-Sham calculation. Finally, as one can see, the first summation runs only over the occupied states (occ) so this contribution to the self-energy is not so demanding.

The expression for the correlation contribution is [70]

$$\langle m, \mathbf{k}| \Sigma^C(E) |l, \mathbf{k}\rangle = \frac{1}{V} \sum_{v}^{\text{occ + unocc}} \sum_{\mathbf{q}}^{\text{BZ}} \sum_{\mathbf{G_1 G_2}} M^{vl}_{\mathbf{G}}(\mathbf{k}, \mathbf{q})[M^{vm}_{\mathbf{G}}(\mathbf{k}, \mathbf{q})]^* \tilde{v}_{\mathbf{G_1 G_2}}(\mathbf{q}) J^{n\mathbf{k}-\mathbf{q}}_{\mathbf{G_1 G_2}}(\mathbf{q}, \omega), \tag{2.51}$$

where $\tilde{v}_{\mathbf{G_1G_2}}(\mathbf{q})$ is the modified Coulomb interaction, which includes local field effects and $J^{n\mathbf{k}-\mathbf{q}}_{\mathbf{G_1G_2}}(\mathbf{q},\omega)$ is a frequency convolution integral, in which the dynamical effects of the correlation are contained. A different energy cut-off could be defined in order to evaluate the double summation over the reciprocal lattice vectors $\mathbf{G_1}$ and $\mathbf{G_2}$. It is important to note that, unlike the exchange contribution to the self-energy, the sum over the band index v should extend up to infinity although in practice only a finite number of states can be used.

Once the self-energy is obtained, the many-body corrections to the single-particle Hamiltonian, that is, the quasiparticle energies, are determined by using the expression [72]

$$E_i = \epsilon_i^{\mathrm{KS}} + Z_i \left\langle \phi_i^{\mathrm{KS}} \right| \Sigma(\epsilon_i^{\mathrm{KS}}) - V_{XC}^{\mathrm{KS}} \left| \phi_i^{\mathrm{KS}} \right\rangle, \tag{2.52}$$

with

$$Z_i^{-1} = 1 - \left\langle \phi_i^{\mathrm{KS}} \right| \frac{d\Sigma}{d\epsilon} \epsilon_i^{\mathrm{KS}} \left| \phi_i^{\mathrm{KS}} \right\rangle, \tag{2.53}$$

where the superscript KS refers to the Kohn-Sham eigenenergies, eigenfunctions and exchange-correlation potential. Note that in equation (2.52) the quasiparticle energies are determined by the Kohn-Sham states. Since the Kohn-Sham equation has the form of one-particle Schrödinger's equation with an effective potential, then one could think of using their eigenstates and eigenvalues for a system where a particle is added or removed. Although, as it is well known, DFT or Kohn-Sham approach understimate the band gap value, the Kohn-Sham eigenfunctions and eigenvalues have been used as approximation, having good results [72].

It is important to say that one, in general, only compute the matrix elements of the self-energy operator for some specific states, in order to keep computational efficiency. Then, is useful to use the Wannier interpolation method to obtain the complete band structure (see Appendix B).

2.6.5 The G_0W_0 or single shot GW approximation

Most current GWA calculations do not attempt a numerically expensive, self-consistent calculation of G and W. One refer to this kind of approach as the G_0W_0 or single shot GW approximation, in which a non self-consistent calculation is performed. The single-particle non-interacting propagator G_0

is constructed with the aid of Kohn-Sham orbitals and energies. Then the RPA polarizability is used to obtain the dielectric function and calculate the screened Coulomb interaction W_0. The self-energy operator is constructed using both G_0 and W_0 and the corrections to the energies are obtained.

In general, compared with DFT computational implementations, GW calculations have slower convergence with respect to the basis size, are more sensitive to the pseudopotential used and have a scaling of the computational running time with system size (as represented by its number of electrons N) as N^4. Concerning the memory and number of CPUs they scale as N^3 or $N^2 \ln N$ [77].

Calculated quasiparticle corrections, using the G_0W_0 approximation, to a DFT band structure agree in general well with experiment [68]. Since self-consistent GWA calculations are computationally very demanding and there exists an increasing discrepancy between theory and experiment upon full self-consistency (here, vertex corrections must be included), inclusion of the self-consistency is not justified due to the increase in computational cost and the loss of predictive power [70]. However, some possible implementations to perform the GWA in current calculations are shown. In Figure 2.3 the procedure to obtain the quasiparticle corrections is shown for a G_0W_0 calculation. In Figure 2.4 the procedure to obtain the quasiparticle corrections is shown for a GW_0 calculation, in which only the propagator G is updated with the quasiparticle corrections of a previous iteration and this is done self-consistently. In Figure 2.5 a complete self-consistent procedure to obtain the quasiparticle corrections is shown; both the propagator G and the screened potential W are updated in every iteration. The self-consistent condition in the last two methods is that the propagator which was constructed using the quasiparticle energies of a previous step, could be constructed with the quasiparticle energies obtained in the present step.

2.7 The Bethe-Salpeter equation

In the case of optical spectra, using the GW approximation without including electron-hole interactions, the redshift band gap problem in a DFT calculation, becomes a blueshift problem. The corrected energies used to calculate the optical response predict that absorption in the material will exist at higher energies that it is in reality. This is not due to a failure of the GW

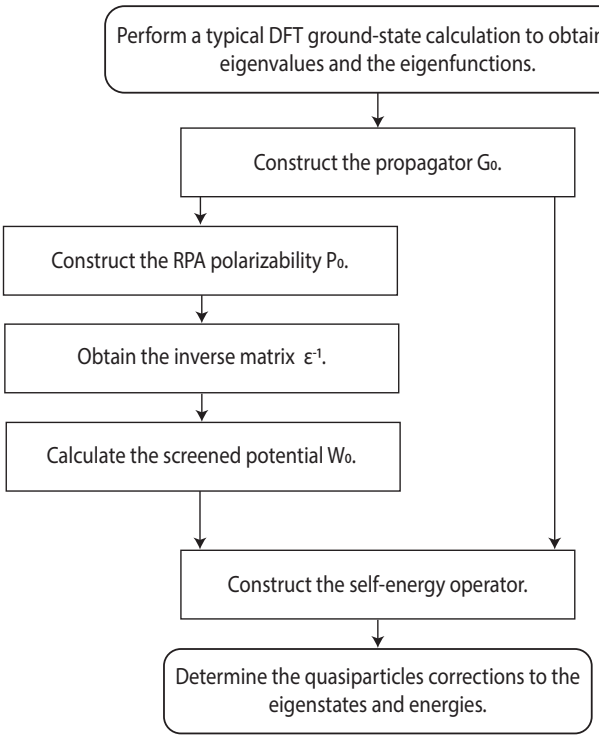

Figure 2.3: Procedure to obtain the quasiparticle corrections for a G_0W_0 calculation.

approach. However, one considers the addition of a hole with respect to the ground state and not, as in the case of absorption, the addition of a hole and then the addition of an electron in the presence of that hole. These effects have been well known for some time, being described by J. Frenkel as excitations waves [78] and developed using the band structure picture by G. Wannier [79].

The Bethe-Salpeter equation (BSE) was derived in 1951 to calculate the ground state of the deuteron [80]. The used methodology was proposed by the authors to *"deal only with two Fermi-Dirac particles interacting with each other by means of an arbitrary (electrodynamic or mesonic) interaction in the absence of any external forces, particles, or quanta."*. The complete derivation is very general cause it is included in the relativity framework, however the authors pointed out that in the nonrelativistic limit and for the case of small coupling constant for the interaction their formalism leads

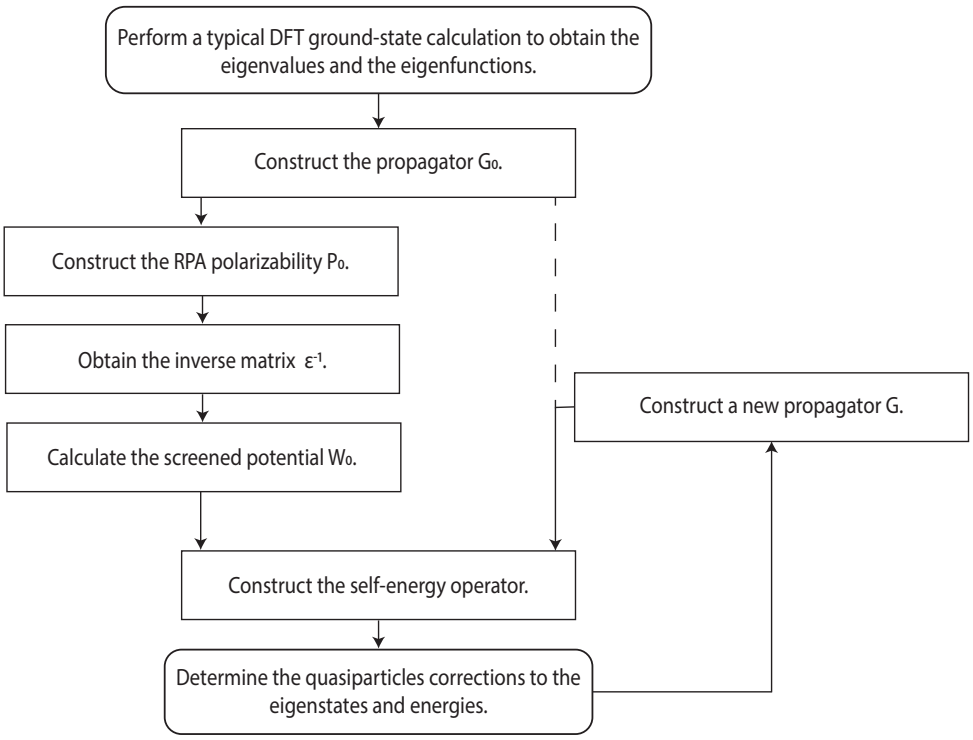

Figure 2.4: Procedure to obtain the quasiparticle corrections for a GW_0 calculation; only the propagator G is updated with the quasiparticle corrections of the previous iteration and this is done self-consistently. The dashed line emphasizes that just for the first iteration the propagator G_0 is required.

exactly to the ordinary nonrelativistic Schrödinger equation for a bound state for two particles.

The BSE is actually found via Green's-function theory [72]. It requires the correct calculation of the quasielectron and the quasihole and contains an interaction term that mixes the formerly independent transitions. The inclusion of the electron-hole interaction by solving the Bethe-Salpeter equation leads to much better overall agreement of the calculated optical response with experiment, predicting correctly the below-band-gap absorption of semiconductors.

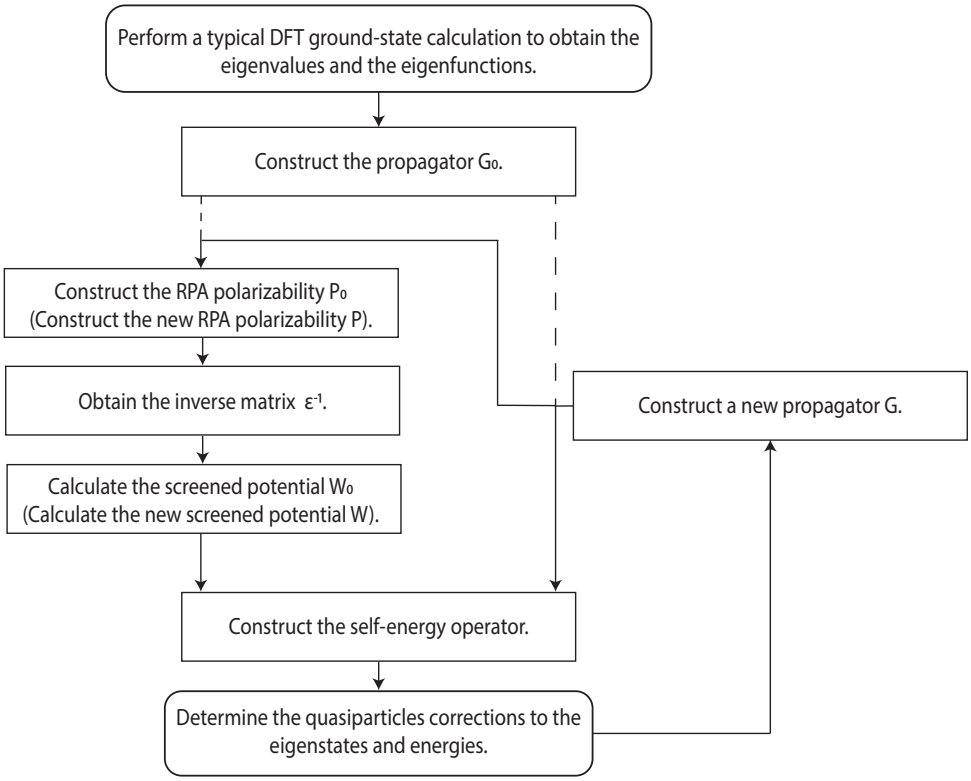

Figure 2.5: Procedure to obtain the quasiparticle corrections for a self-consistent GW calculation; both the propagator G and the screened potential W are updated with the quasiparticle corrections of the previous iteration. The dashed line emphasizes that just for the first iteration the propagator G_0 is required.

2.7.1 Excitons

Reflectance and absorption spectra often show non zero values for photon energies below the energy band gap, where we might expect the crystal to be transparent. This below-band-gap absorption results from the creation of a bound electron-hole pair. An electron and a hole may be bound together by their attractive Coulomb interaction, just as an electron is bound to a proton to form a neutral hydrogen atom. The bound electron-hole pair is a quasiparticle called an exciton. An exciton can be formed in every insulating crystal and move trough it transporting energy; but do not transport charge because it is electrically neutral [63]. A free electron and hole are created

whenever a photon with energy greater than the energy gap value is absorbed in a crystal. In the formation of excitons, the energy states are lowered with respect to the band gap due to the binding energy of the exciton (Figure 2.6).

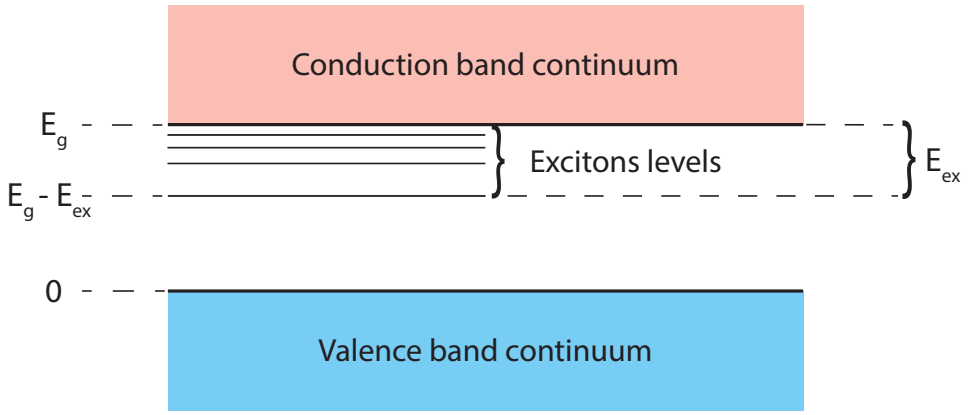

Figure 2.6: Energy levels of an exciton created in a direct process. E_g corresponds to the energy band gap. The binding energy of the exciton is E_{ex}, referred to a free electron and hole. Hence, the lowest energy absorption line of the crystal at absolute zero is $E_g - E_{ex}$.

2.7.2 The Bethe-Salpeter equation

The Bethe-Salpeter approach to the calculation of two-particle excited states is a straightforward extension of the GW approach for the calculation of one-particle excited states and it leads to an effective two-particle Hamiltonian [72].

The BSE can be written in the form [81]

$$\begin{aligned} L(12;1'2') =& L_0(12;1'2') \\ &+ \int \mathrm{d}(3456) L_0(14;1'3') K(35;46) L(62;52'), \end{aligned} \tag{2.54}$$

where $L(12;1'2')$ is the electron-hole correlation function and $K(35;46)$ is the electron-hole interaction kernel.

$$L_0(12;1'2') = G(1,2')G(2,1') \tag{2.55}$$

corresponds to free electron-hole pairs with no interaction. L has a time dependency, contained in the set of variables denoted with numbers, but a Fourier transform can be performed in order to express it in the frequency domain; L_0 can be written as

$$L_0(12,1'2';\omega) = i\sum_{v,c}\left[\frac{\psi_c(\mathbf{x_1})\psi_v^*(\mathbf{x_1'})\psi_v(\mathbf{x_2})\psi_c^*(\mathbf{x_2'})}{\omega-(E_c-E_v)} - \frac{\psi_v(\mathbf{x_1})\psi_c^*(\mathbf{x_1'})\psi_c(\mathbf{x_2})\psi_v^*(\mathbf{x_2'})}{\omega+(E_c-E_v)}\right], \tag{2.56}$$

where v runs over the occupied hole states and c over the empty electron states. The electron-hole correlation function can also be written in similar form to this latter equation [81]

$$L(12,1'2';\omega) = i\sum_{S}\left[\frac{\chi_S(\mathbf{x_1},\mathbf{x_1'})\chi_S^*(\mathbf{x_2'},\mathbf{x_2'})}{\omega-\Omega_S} - \frac{\chi_S(\mathbf{x_2},\mathbf{x_2'})\chi_S^*(\mathbf{x_1'},\mathbf{x_1})}{\omega-\Omega_S}\right], \tag{2.57}$$

where χ_S is the electron-hole amplitude corresponding to excitations energies Ω_S, given by

$$\chi_S(\mathbf{x},\mathbf{x'}) = -\langle N,0|\,\psi^\dagger(\mathbf{x'})\psi(\mathbf{x})\,|N,S\rangle \tag{2.58}$$

and S refers to the correlated electron-hole excitations of the system. Transforming all continuous position variables into the basis given by the single-particle wave functions of the electron and hole states, the electron-hole amplitude can be expressed in the form

$$\chi_S(\mathbf{x},\mathbf{x'}) = \sum_{v}^{\text{occ}}\sum_{c}^{\text{empty}}\left(A_{vc}^S\psi_c(\mathbf{x})\psi_v^*(\mathbf{x}') + B_{vc}^S\psi_v(\mathbf{x})\psi_c^*(\mathbf{x}')\right). \tag{2.59}$$

In equation (2.59), the sums only run over occupied (v) and empty states (c), respectively.

Using equation (2.59) and substituing equations (2.56) and (2.57) into the BSE (2.54), the following coupled equations for A_{vc}^S and B_{vc}^S are found

$$(E_c-E_v)A_{vc}^S + \sum_{v'c'}K_{vc,v'c'}^{AA}(\Omega_S)A_{v'c'}^S + \sum_{v'c'}K_{vc,v'c'}^{AB}(\Omega_S)B_{v'c'}^S = \Omega_S A_{vc}^S, \tag{2.60}$$

$$\sum_{v'c'} K^{BA}_{vc,v'c'}(\Omega_S)A^S_{v'c'} + (E_c - E_v)B^S_{vc} + \sum_{v'c'} K^{BB}_{vc,v'c'}(\Omega_S)B^S_{v'c'} = \Omega_S B^S_{vc}. \quad (2.61)$$

where $K^{ab}_{vc,v'c'}$ are interaction matrix elements, and a and b can be A or B. It has been shown that the off-diagonal components given by K^{AB} and K^{BA} are small with negligible contribution to the excitation energies [81]. Hence, setting $K^{BA} = K^{AB} = 0$ (2.60) and (2.61) are decoupled into two eigenvalue equations for A^S_{vc} and B^S_{vc}, yielding exactly the same excitations. However, the solutions for B give excitation energies with negative sign. The eigenvalue equation for A^S_{vc} with positive energies are given by

$$(E_c - E_v)A^S_{vc} + \sum_{v'c'} K^{AA}_{vc,v'c'}(\Omega_S)A^S_{v'c'} = \Omega_S A^S_{vc}, \quad (2.62)$$

which is equivalent to expanding the excited states in electron-hole pair configurations as

$$|N,S\rangle = \sum_{v}^{\text{hole}} \sum_{c}^{\text{elec}} A^S_{vc}\hat{a}^\dagger_v \hat{b}^\dagger_c |N,0\rangle = \sum_{v}^{\text{hole}} \sum_{c}^{\text{elec}} A^S_{vc} |vc\rangle , \quad (2.63)$$

where $\hat{a}^\dagger_v$ and $\hat{b}^\dagger_c$ are the hole and electron creation operators, respectively. The expansion of the excited states given in equation 2.63 is possible due to the consideration of non diagonal terms of the electron-hole kernel K^{BA} and K^{AB} equal to zero, which is called the Tamm-Dancoff approximation.

Now, is necessary to focus on the kernel K. The matrix elements of the electron-hole interaction kernel are given by

$$K^{AA}_{vc,v'c'}(\Omega_S) = i \int \mathrm{d}(3456)\psi_v(\mathbf{x_4})\psi^*_c(\mathbf{x_3})K(35;46;\Omega_S)\psi^*_{v'}(\mathbf{x_5})\psi_{c'}(\mathbf{x_6}), \quad (2.64)$$

with a similar expression for K^{BB}. The electron-hole interaction kernel is given by the functional derivative

$$K(35;46) = \frac{\delta\left[v(3)\delta(3,4) + \Sigma(3,4)\right]}{\delta G(6,5)}. \quad (2.65)$$

In order to be consistent with the quasiparticle calculation, the GWA is employed for the self-energy operator. Ignoring the derivative of W with respect to G one obtains

$$K(35;46) = -i\delta(3,4)\delta(5^-,6)v(3,6) + i\delta(3,6)\delta(4,5)W(3^+,4) \quad (2.66)$$

$$=: K^x(35;46) + K^d(35;46). \tag{2.67}$$

where K^x is the exchange term, which results from the Coulomb potential and it is responsible, for instance, of the splitting between spin excitations, and in turn this would be reflected on the excitation spectrum. K^d is the kernel contribution that results from the screened-exchange self-energy. It is a direct interaction term that describes the attractive nature of the electron-hole interaction and thus the formation of bound electron-hole states or excitons [81]. The frequency dependency of the kernel is given in the direct term trough the screened Coulomb interaction W.

The matrix elements of the interaction kernel are given by [81]

$$\begin{aligned}\langle vc|\, K^{AA,d}(\Omega_S)\,|v'c'\rangle = &\int \mathrm{d}\mathbf{x}\mathrm{d}\mathbf{x}'\psi_c^*(\mathbf{x})\psi_{c'}(\mathbf{x})\psi_v(\mathbf{x}')\psi_{v'}^*(\mathbf{x}') \\ &\times \frac{1}{2\pi}\int \mathrm{d}\omega \mathrm{e}^{-i\omega 0^+} W(\mathbf{r},\mathbf{r}',\omega) \\ &\times \left[\frac{1}{\Omega_S - \omega - (E_{c'}^{QP} - E_v^{QP}) + i0^+}\right. \\ &\left. + \frac{1}{\Omega_S + \omega - (E_c^{QP} - E_v^{QP}) + i0^+}\right]\end{aligned} \tag{2.68}$$

and

$$\langle vc|\, K^{AA,x}(\Omega_S)\,|v'c'\rangle = \int \mathrm{d}\mathbf{x}\mathrm{d}\mathbf{x}'\psi_c^*(\mathbf{x})\psi_v(\mathbf{x})v(\mathbf{r},\mathbf{r}')\psi_{c'}^*(\mathbf{x}')\psi_{v'}^*(\mathbf{x}'). \tag{2.69}$$

The matrix elements consist of six-dimensional real-space integrals involving the quasiparticle electron and hole eigenenergies and eigenfunctions. In the case of equation (2.68) it is also required a frequency integration. For this, the screened Coulomb interaction can be expanded in a plasmon-pole model as

$$W(\mathbf{r},\mathbf{r}',\omega) = \sum_l W_l(\mathbf{r},\mathbf{r}')\frac{\omega_l}{2} \times \left(\frac{1}{\omega - \omega_l + i0^+} - \frac{1}{\omega + \omega_l - i0^+}\right), \tag{2.70}$$

where ω_l denotes the plasmon frequency and $W_l(\mathbf{r},\mathbf{r}')$ the spatial behavior of the plasmon of mode l. Substituing equation (2.70) in (2.68) gives

$$\langle vc|\, K^{AA,d}(\Omega_S)\,|v'c'\rangle = \sum_l \int \mathrm{d}\mathbf{x}\mathrm{d}\mathbf{x}'\psi_c^*(\mathbf{x})\psi_{c'}(\mathbf{x})\psi_v(\mathbf{x}')\psi_{v'}^*(\mathbf{x}')W(\mathbf{r},\mathbf{r}')$$

$$\times \frac{\omega_l}{2}\left[\frac{1}{\omega_l-(\Omega_S-(E_{c'}^{QP}-E_v^{QP}))}-\frac{1}{\omega_l-(\Omega_S-(E_c^{QP}-E_v^{QP}))}\right] \quad (2.71)$$

which is an expression that can be evaluated analitically.

In many cases, the excitations $|S\rangle$ are mainly composed from electron-hole pair configurations $|vc\rangle$ whose transition energies $(E_c^{QP}-E_v^{QP})$ are close to the excitation energy Ω_S, so the difference $\Omega_S-(E_c^{QP}-E_v^{QP})$ are much smaller than the plasmon frequencies ω_l, so can they be considered as zero. With this consideration, equation (2.71) can be replaced by

$$\langle vc|\, K^{AA,d}\,|v'c'\rangle = \int \mathrm{d}\mathbf{x}\mathrm{d}\mathbf{x}'\psi_c^*(\mathbf{x})\psi_{c'}(\mathbf{x})\psi_v(\mathbf{x}')\psi_{v'}^*(\mathbf{x}')W(\mathbf{r},\mathbf{r}',\omega=0), \quad (2.72)$$

which ignores de dinamically screening effects.

2.7.3 Optical spectrum in periodic systems

In periodic systems, such as crystals, the single-particle states are now given by $|\psi_{n\mathbf{k}}\rangle$ with the wave vector $\mathbf{k}$ in the first Brillouin zone. Thus, the two-particle excitations of equation (2.63) are now written as

$$|N,S\rangle = \sum_{\mathbf{k}}^{\text{hole}}\sum_{v}^{\text{elec}}\sum_{c} A_{vc\mathbf{k}}^S \hat{a}_{v\mathbf{k}}^\dagger \hat{b}_{c,\mathbf{k}+\mathbf{Q}}^\dagger\,|N,0\rangle = \sum_{\mathbf{k}}^{\text{hole}}\sum_{v}^{\text{elec}}\sum_{c} A_{vc}^S\,|vc\mathbf{k}\rangle\,, \quad (2.73)$$

where $\mathbf{Q}$ is the total momentum of the two-particle state. In an optical excitation process, $\mathbf{Q}$ is the momentum of the photon that is absorbed by the two-particle state.

The eigenvalue problem of equation (2.62) now is transformed into [81]

$$(E_{c,\mathbf{k}+\mathbf{Q}}^{QP}-E_{v\mathbf{k}}^{QP})A_{vc\mathbf{k}}^S + \int_{V_{BZ}}\mathrm{d}^3\mathbf{k}'\sum_{v',c'}\langle vc\mathbf{k}|\, K\,|v'c'\mathbf{k}'\rangle\, A_{v'c'\mathbf{k}'}^S = \Omega_S A_{vc\mathbf{k}}^S, \quad (2.74)$$

where $\langle vc\mathbf{k}| K |v'c'\mathbf{k}'\rangle$ are the matrix elements of the electron-hole interaction kernel. The energy difference $(E^{QP}_{c,\mathbf{k}+\mathbf{Q}} - E^{QP})$ is given by the quasiparticle corrections calculated with the GWA. The integral over $\mathbf{k}$ is performed over the volume of the first Brillouin zone. In semiconductor crystals, several occupied and unoccupied bands v and c, as well as several (hundreds) wave vectors $\mathbf{k}$ are necessary to represent the transitions relevant to the optical spectrum.

The measurable quantity that can be obtained with this formalism is the macroscopic transverse dielectric function of the system, whose imaginary part is given by [81]

$$\epsilon_2(\omega) = \frac{16\pi e^2}{\omega^2} \sum_S \left| \hat{\lambda} \cdot \langle 0| \mathbf{v} |S\rangle \right|^2 \delta(\omega - \Omega_S). \tag{2.75}$$

where $\hat{\lambda} = \frac{\mathbf{A}}{|\mathbf{A}|}$ is the unitary polarization vector of the light and $\mathbf{v} = \frac{i}{\hbar}[H, \mathbf{r}]$ is the single-particle velocity or current operator. The optical transition matrix elements are given by

$$\langle 0| \mathbf{v} |S\rangle = \sum_v^{\text{hole}} \sum_c^{\text{elec}} A^S_{vc} \langle v| \mathbf{v} |c\rangle . \tag{2.76}$$

It is important to mention that, in the calculation of $\epsilon(\omega)$, the inclusion of local fields effects, i.e., response fields of the crystal that tend to screen the electric field, results in a significant reduction of the dielectric function. Equation (2.75) already includes these effects [82].

Without considering electron-hole interactions, the excitations are given by transitions between independent hole and electron states, so equation (2.75) reduces to [81]

$$\epsilon^0_2(\omega) = \frac{16\pi e^2}{\omega^2} \sum_{v,c} \left| \hat{\lambda} \cdot \langle v| \mathbf{v} |c\rangle \right|^2 \delta(\omega - (E_c - E_v)), \tag{2.77}$$

where v (c) denotes valence (conduction) states.

2.7.4 Solving the problem from first principles

The procedure begins with a ground-state calculation using the Kohn-Sham approach to obtain the energy eigenvalues and the eigenfunctions of the system. With these elements one can construct the propagator G_0. Then, one

can determine the RPA polarizability and calculate the screened potential W_0. Using the GWA one can, with both G_0 and W_0, construct the self-energy operator and thus the quasiparticles corrections to the states can be calculated. The electron-hole interaction kernel K is determined with the aid of W_0. Finally, using the kernel and the quasiparticle corrections one can solve the BSE and then obtain the macroscopic dielectric function. This procedure is schematized in Figure 2.7. The main equations, used to evaluate the specified quantities at every step, are displayed with their corresponding number.

(1)

$$G_0(\mathbf{r}, \mathbf{r}'; E) = \sum_i \frac{\phi_i(\mathbf{r})\phi_i^*(\mathbf{r}')}{E - \epsilon_i}.$$

(2)

$$P(1,2) = -iG(1,2)G(2,1).$$

(3)

$$\epsilon_{\mathbf{G},\mathbf{G}'}(\mathbf{q};\omega) = \delta_{\mathbf{G},\mathbf{G}'} - \frac{4\pi}{|\mathbf{q}+\mathbf{G}|^2} P_{\mathbf{G},\mathbf{G}'}(\mathbf{q};\omega).$$

(4)

$$W_{\mathbf{G},\mathbf{G}'}(\mathbf{q};\omega) = \frac{4\pi}{|\mathbf{q}+\mathbf{G}|^2} \epsilon^{-1}_{\mathbf{G},\mathbf{G}'}(\mathbf{q};\omega).$$

(5)

$$\Sigma(1,2) = iG(1,2)W(1^+,2).$$

(6)

$$K(35;46) = -i\delta(3,4)\delta(5^-,6)v(3,6) + i\delta(3,6)\delta(4,5)W(3^+,4),$$
$$=: K^x(35;46) + K^d(35;46).$$

(7)

$$E_i = \epsilon_i^{KS} + Z_i \left\langle \phi_i^{KS} \right| \Sigma(\epsilon_i^{KS}) - V_{XC}^{KS} \left| \phi_i^{KS} \right\rangle$$

with

$$Z_i^{-1} = 1 - \left\langle \phi_i^{KS} \right| \frac{d\Sigma}{d\epsilon} \epsilon_i^{KS} \left| \phi_i^{KS} \right\rangle .$$

(8)

$$(E_{c,\mathbf{k}+\mathbf{Q}}^{QP} - E_{v\mathbf{k}}^{QP}) A_{vc\mathbf{k}}^S + \int_{V_{BZ}} \mathrm{d}^3\mathbf{k}' \sum_{v',c'} \langle vc\mathbf{k}| K |v'c'\mathbf{k}'\rangle A_{v'c'\mathbf{k}'}^S = \Omega_S A_{vc\mathbf{k}}^S.$$

(9)

$$\epsilon_2(\omega) = \frac{16\pi e^2}{\omega^2} \sum_S \left| \hat{\lambda} \cdot \langle 0| \mathbf{v} |S\rangle \right|^2 \delta(\omega - \Omega_S)$$

with

$$\langle 0| \mathbf{v} |S\rangle = \sum_v^{\text{hole}} \sum_c^{\text{elec}} A_{vc}^S \langle v| \mathbf{v} |c\rangle .$$

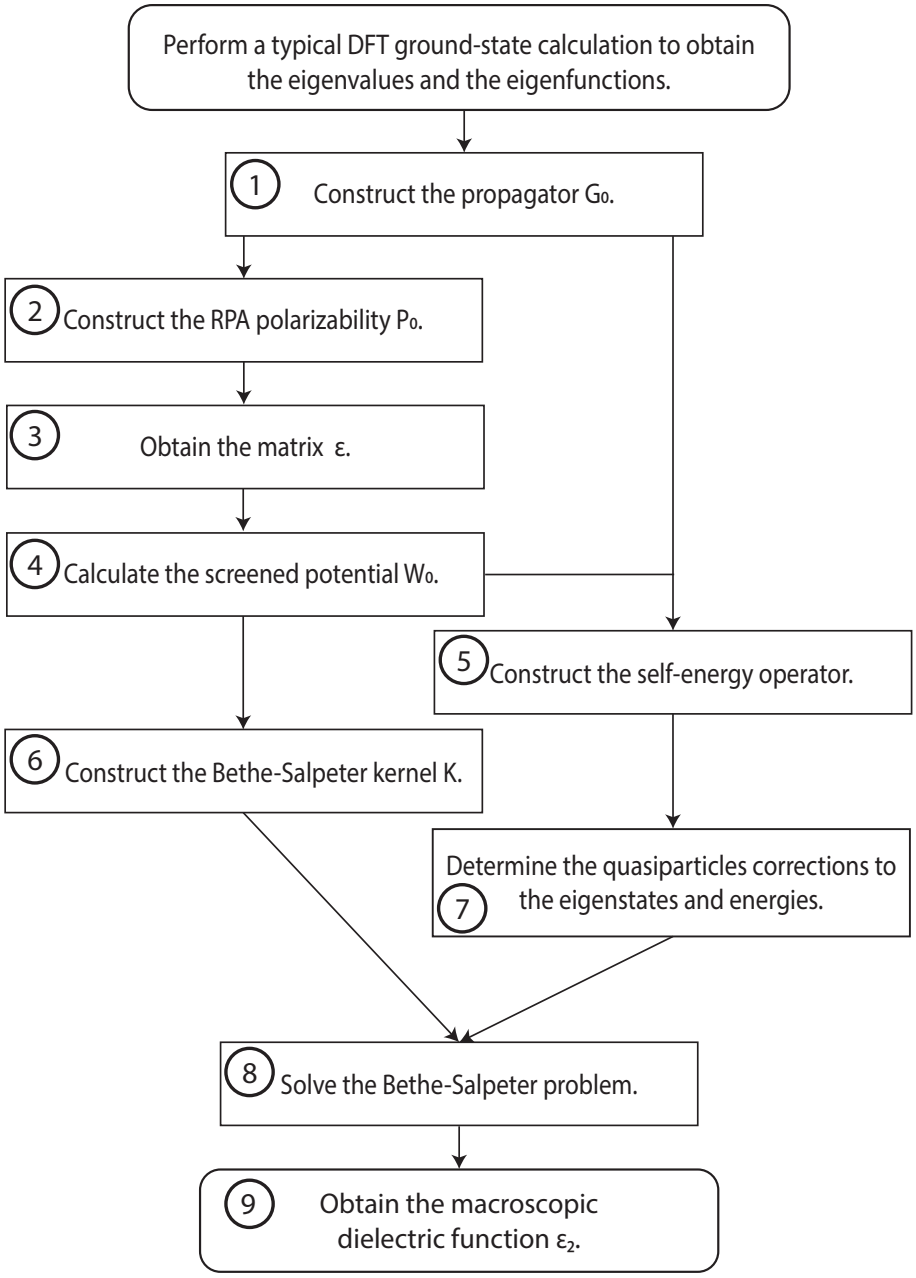

Figure 2.7: Flow chart describing the procedure for obtaining the macroscopic dielectric function considering excitonic effects within the Bethe-Salpeter formalism on top of the G_0W_0 approximation.

Chapter 3

Results and discussion

In this chapter, the numerical results, obtained by performing the corresponding calculations, of the crystalline and electronic structure and optical properties of blue phosphorene are presented. The electronic structure calculated within the Kohn-Sham approach and with the corresponding GW corrections (using the Wannier interpolation method) are obtained and compared. The spectrum of linear optical response is calculated within the independent-particle approach and using the Bethe-Salpeter equation, in order to include excitonic effects in the spectrum. The obtained results are compared with previous works.

The ABINIT software (see Appendix C) was employed for the calculations. The Wannier90 software (see Appendix B) was employed to obtain the quasiparticle band structure.

3.1 Crystalline structure

The atomic positions in the primitive cell were necessary to begin with the ground state calculation and, then, to obtain the properties in which we are interested in. In this case, the relaxed crystalline structure was obtained in a previous work [49]; those atomics positions were used here to represent the atomic system correctly. The considerations related to obtain the correct atomic positions, in that work, were the following.

The supercell approximation was selected to deal with the aperiodic configu-

ration of the blue phosphorene monolayer. Also, the spin-orbit coupling was neglected, due to that phosphorus could be considered as a light element. The Perdew-Burke-Ernzerhof (PBE) exchange-correlation potential was selected. This is an exchange-correlation potential characteristic of a GGA which has been used for DFT calculations.

A convergence study atomic structure was performed as a function of the energy cut-off, the number of **k** points in reciprocal space and the interatomic distance between blue phosphorene monolayers. In general, one select an specific value for all parameters and then one can vary just one of them at a time, keeping the others constant, until convergence is reached. This process is repeated by keeping the value of the corresponding parameter at which convergence was reached in the previous step and varying of a second parameter. There is no specific order to perform a convergence study in general. In this case, when I speak of a converged structure value, I refer to that at which the difference in total energy of the system of the last two steps of the convergence study is less than some criterion. In the case of this study, for the relaxed or ground state structure, the energy change criterion was of 1×10^{-5} Ha. So, if the change in energy between the last two steps was less than this value, the convergence of the structure was said to be obtained.

The unit cell of blue phosphorene is shown in Figure 1.3. As initial approximation, the atomic positions where those of the ideal hexagonal structure. The number of **k** points in reciprocal space were varied using the Monkhorst-Pack methodology [83, 84] and the converged grid was that of $12 \times 12 \times 1$. Then the distance between monolayers, due to the supercell modeling, was obtained as 25 Å. Finally, the energy cut-off was selected as 35 Ha. The optimal structure was obtained by minimizing the forces between the atoms until every cartesian component of the force tensor in the unit cell were less than 1×10^{-9} Ha/Bohr. In Figure 3.1a the top (XY plane) and lateral (XZ plane) views of the relaxed blue phosphorene structure are shown. In Table 3.1, there is a comparison between the obtained values for the cell parameters of the studied structure and those reported elsewhere. It is notorious that the obtained lattice values are comparable with those already reported.

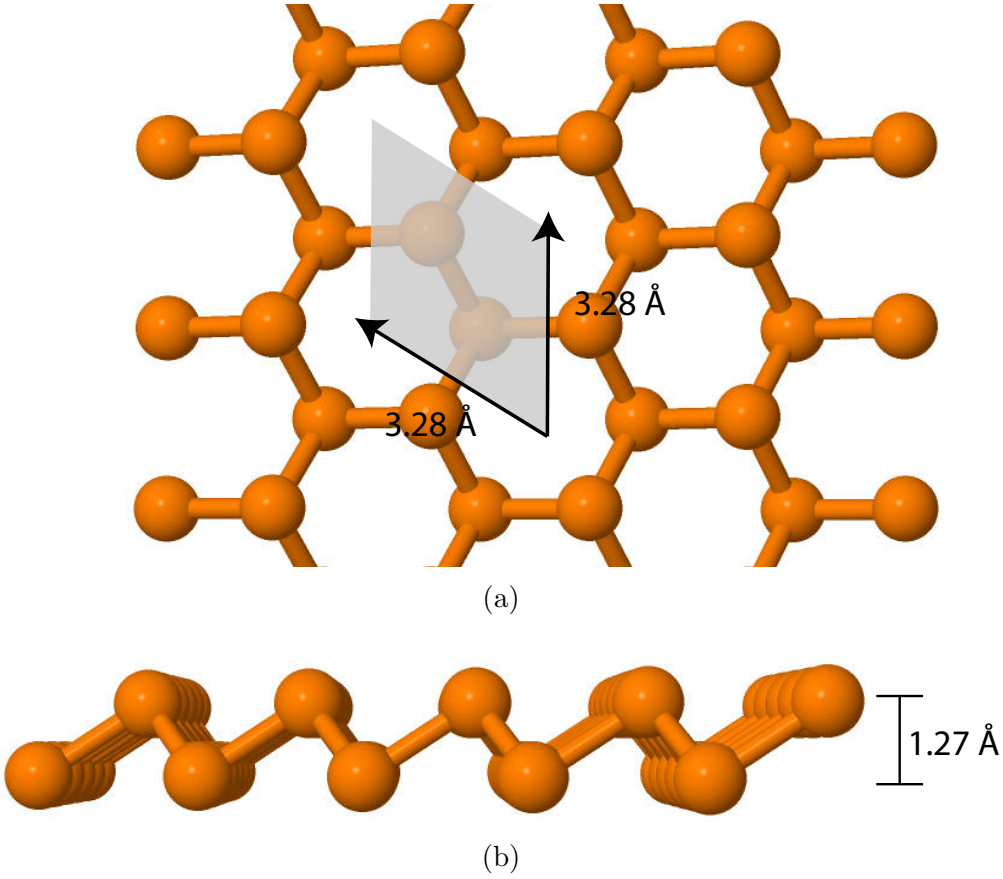

(a)

(b)

Figure 3.1: (a) Top and lateral (b) view of the monolayer of blue phosphorene. The lateral view shows the zig zag array of the atoms. The shaded region represents the primite cell.

3.2 Electronic structure

To obtain the band structure of the blue phosphorene monolayer, described in 3.1 in the Kohn-Sham approach, the same values determined in the convergence studies were used. But, in this case, the number of **k** points in reciprocal space was selected as 120, being sufficient to obtain the appropriate smoothed bands. These points were along the path delimited by the high-symmetry points M-Γ-K-M in the first Brillouin zone, as is shown in Figure 1.5. Even more, this path delimits the irreducible Brillouin zone,

Table 3.1: Comparison of the obtained structural parameters of the monolayer of blue phosphorene reported in other works.

	Approximation for E_{XC}	**Magnitude of a_1 (Å)**	**Bonding distance (Å)**	**d (Å)**	**Angle between bonds (degrees)**
[49]	GGA-PBE	3.28	2.27	1.27	92.80
[41]	GGA-PBE	3.33	2.27		
[55]	GGA-HSE06		2.27	1.24	92.88
[59]	GGA-PBE	3.33			
[58]	GGA-PBE	3.28		1.24	
[85]	GGA-PBE	3.28		1.24	
[86]	GGA-PBE		2.26	1.23	93.07
[87]	GGA-PBE	3.29		1.20	

which is the smallest fraction of the Brillouin zone that is sufficient to determine all the information on the excitations of the crystal. The excitations at all other $\mathbf{k}$ points outside the irreducible Brillouin zone are related by the symmetry operations.

In Figure 3.2 the band structure is shown. Blue phosphorene has an indirect band gap of 1.92 eV. This means that electrons in the top of the valence band, which here is set to zero, not only need to gain that amount of energy but also a corresponding change in momentum to pass to the conduction band minimum. Qualitatively, the shape of the bands is very similar, compared with other studies [46, 86], where the reported values for the band gap were of 1.9 eV and 2.098 eV, respectively.

For the single shot GW corrections (G_0W_0) of the bands, a different set of convergence studies was performed. First, the energy cut-off, represented in ABINIT with the parameter ecut was allow to varied; it was determined that the value of 35 Ha was sufficient. Then, the number of bands (nband) obtained to generate the RPA polarizability in the independent-particle approach (equation (2.47) and the self-energy (see equations (2.50) and (2.51)) was 100. The energy cut-off for the correlation part of the self-energy and P_0 (ecuteps) (equations (2.47) and (2.51)) was determined as 5 Ha. The energy cut-off for the exchange part (ecutsigx) of the self-energy operator (equation (2.50)) was of 8 Ha. Finally, the $\mathbf{k}$ point grid was $18 \times 18 \times 1$, which permits a correction for 37 points inside the irreducible Brillouin zone for the first ten

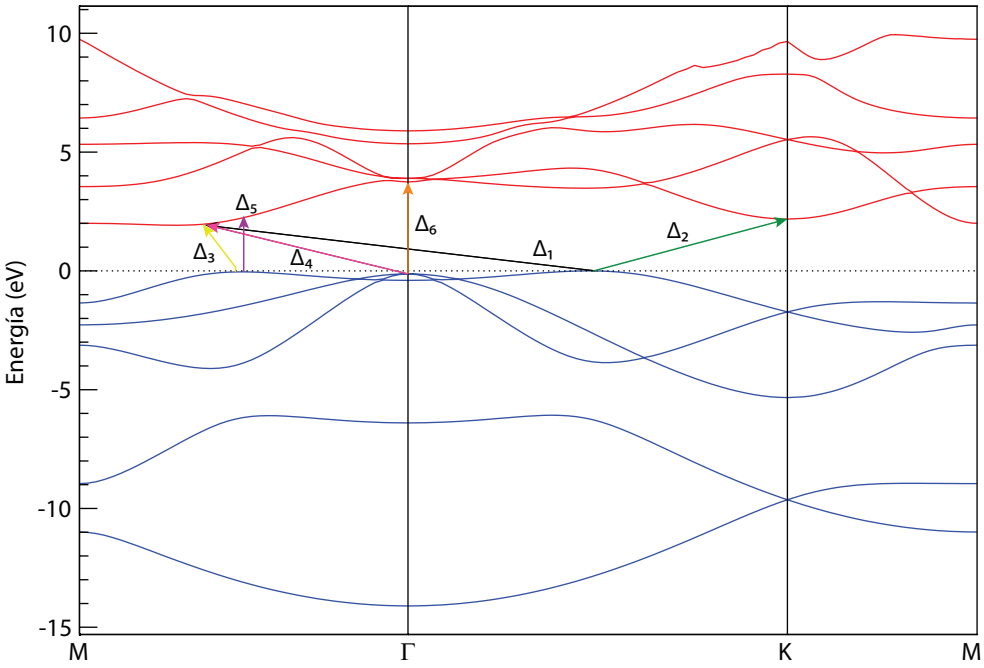

Figure 3.2: Band structure of the blue phosphorene monolayer obtained within the Kohn-Sham approach. The energy band gap is indirect and is marked with the arrow and denoted with the transition Δ_1. The obtained value for the band gap was of 1.92 eV.

bands. The criterion for convergence was that the difference in the corrected band gap value between two steps were less than 10 meV. An important note has to be made: it was mandatory to use this specific grid to obtain the desire corrections for the high-symmetry points; the convergence was accomplish with a grid of $16 \times 16 \times 1$ or 30 points, but due to the Monkhorst-Pack methodology, used to map the reciprocal space by the software, no high-symmetry points were considered within this grid. The corrected band gap value was of 3.44 eV. A summary of the used values, obtained from the convergence tests, in comparison with other works is presented in Table 3.2. The reported convergence values are similar in some cases, as that of the energy cut-off, but presents differences related to the number of included bands and the **k**-point grid. Even though the obtained values may differ, the band-gap value is comparable, which is a proof of correspondence in the methodology.

The quasiparticle band structure was obtained using the Wannier interpo-

Table 3.2: Comparison of the convergence values and the GW energy band gap obtained in this work with those reported by other authors.

	ecut **(Ha)**	nband $\mathbf{P_0}$	nband $\mathbf{\Sigma}$	ecuteps **(Ha)**	ecutsigx **(Ha)**	**k-point grid**	**Band Gap (eV)**
This work	35	100	100	5	8	$18 \times 18 \times 1$	3.44
[88]	25	100	100	11.94	17.64	$12 \times 12 \times 1$	2.95
[89]	18.38					$10 \times 10 \times 1$	3.34
[90]	30	500	500	5		$30 \times 30 \times 1$	3.41
[91]	30	256	480			$18 \times 18 \times 1$	3.53
[92]	30	300	300			$18 \times 18 \times 1$	3.36

lation method (see Appendix B). For this, the Wannier90 software (see last section of Appendix B), inside ABINIT, was used. The corrected 37 points for the ten bands were interpolated to 324 points for the same ten bands. As initial projections, sp^3 and s orbitals were used, following the theoretical description of the bonding in blue phosphorene [47, 93]. The criterion to determine if we are using localized Wannier functions is

$$\langle w_{n\mathbf{0}}(\mathbf{r})|\,\mathbf{r}^2\,|w_{n\mathbf{0}}(\mathbf{r})\rangle - (\langle w_{n\mathbf{0}}(\mathbf{r})|\,\mathbf{r}\,|w_{n\mathbf{0}}(\mathbf{r})\rangle)^2 < 5\mathring{A}^2, \tag{3.1}$$

which is referred as the spread value, and evaluated for every band [94]. In this case, this criterion was accomplished only for the first eight bands. Hence, the Wannier interpolation of quasiparticle bands is shown in Figure 3.3. The maximum valence band was set to zero.

In Table 3.3, a comparison between different energy gaps, represented by Δ_1-Δ_6 in Figure 3.2 and 3.3, is shown. As was mentioned before, the fundamental gap obtained in the DFT approach was of 1.92 eV for the transition Δ_1. The quasiparticle corrections not only changes the energy band-gap value but the position in the first Brioullin zone, given by the transition Δ_4. Considering this, and that the energy differences between the DFT and the GW values are not equal for every transition; as an approximation a GW energy correction at just one point in the first Brioullin zone can be taken, resulting in a rigid shift of the complete band structure.

In Figures 3.4 and 3.5, a comparison between both standard DFT and GW corrected band structures is presented. In both figures, the blue bands represent the DFT valence bands, the red ones are the DFT conduction bands and the purple dotted lines are both the valence and conduction bands corrected

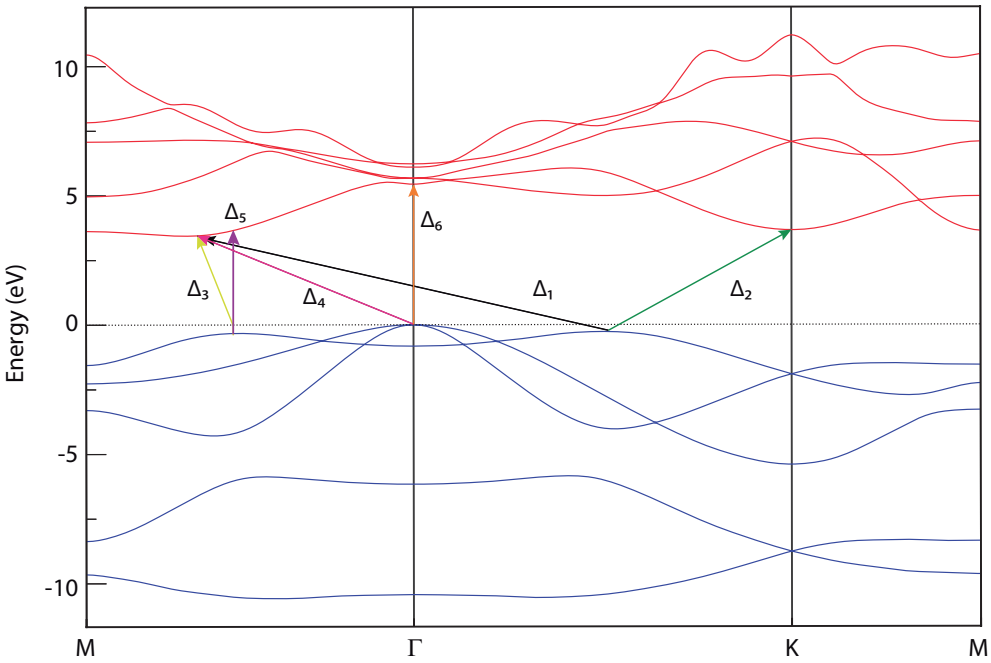

Figure 3.3: Quasiparticle band structure of the blue phosphorene monolayer. The energy band gap is still indirect and denoted with the transition Δ_4. The obtained value for the band gap was of 3.44 eV.

Table 3.3: Comparison between different energy gaps obtained for DFT and GW calculations.

Transition	**DFT Value (eV)**	**GW Value (eV)**	**Difference (eV)**
Δ_1	1.92	3.71	1.79
Δ_2	2.18	3.93	1.75
Δ_3	1.96	3.76	1.80
Δ_4	2.05	3.44	1.39
Δ_5	2.28	4.04	1.76
Δ_6	3.87	5.43	1.56

with the GWA. Figure 3.5 is a zoom of the direct band gap zone to compare easily both band structures.

As was said before, the convergence value for the spread in the Wannier

interpolation was not accomplished for the ninth and tenth bands, so one could not considered that they are represented correctly in the band structure. However, those two bands are not neccesary in this case to discuss the results. For the other eight bands, one can assure that they do are real quasiparticle bands. In Figure 3.5 is easy to see the main differences around the band gap. In the DFT calculation it is predicted that the valence band maximum is at a point between Γ and K. But, for the quasiparticle structure, the valence band maximum is at the Γ point. This new maximum in the valence bands is what gives the change in the position of the fundamental transition in the first Brillouin zone.

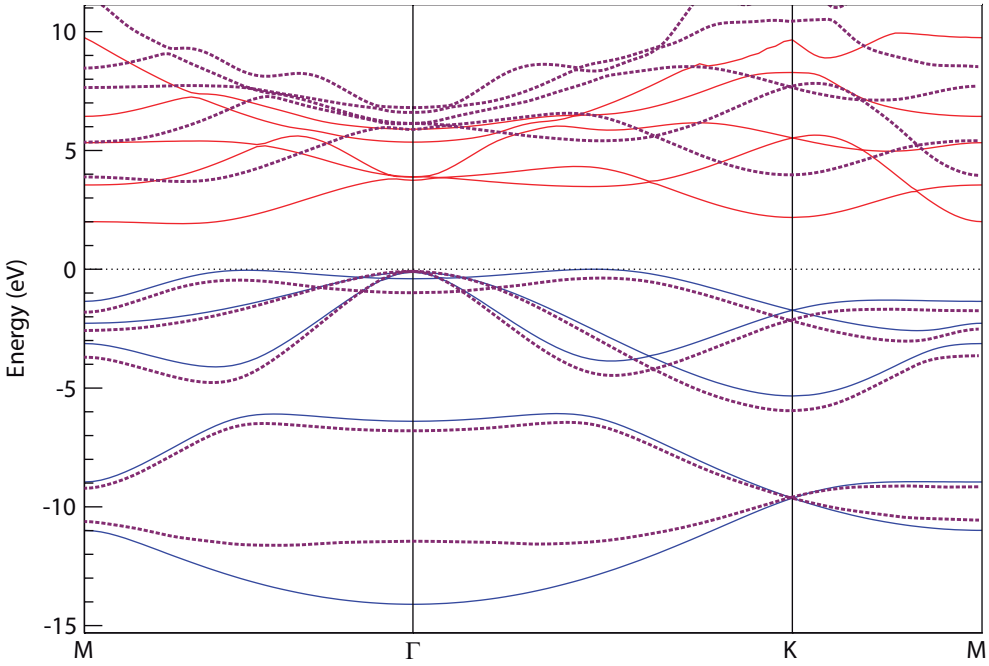

Figure 3.4: Comparison between the DFT standard calculation band structure (red and blue lines) and tha GWA corrected bands (purple dotted lines).

3.3 Optical properties

To obtain the BSE optical spectrum, a new convergence study for both ecut and ecuteps must be performed to see if the used values for the GW correc-

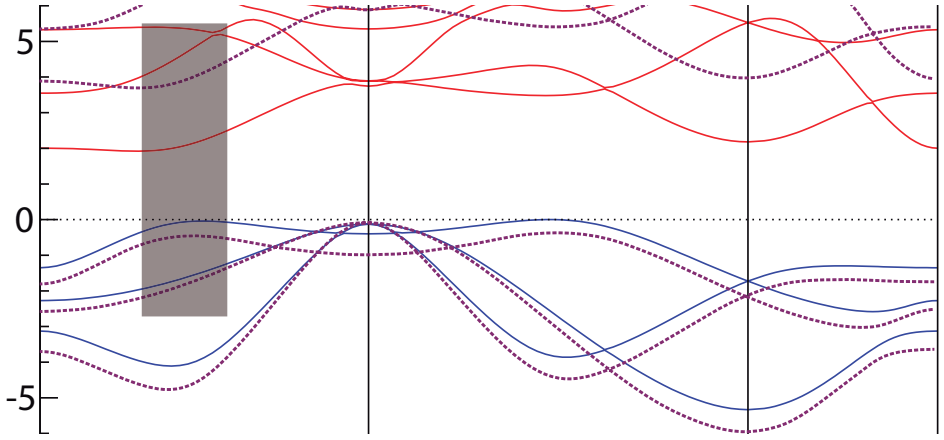

Figure 3.5: Comparison between DFT standard calculation band structure (red and blue lines) and GWA corrected bands (purple dotted lines). This zoom-in view allows one to compare more easily both band structures around the band gap. The shaded region corresponds to the direct transitions that are responsible of the resonance (at around 4 eV) in the optical response of blue phosphorene.

tions could be reduced and thus the computational effort. The parameter ecut, as said before, controls the energy-cutoff to solve the Kohn-Sham equations. The parameter ecuteps is necessary to construct the direct part of the Bethe-Salpeter kernel (equation (2.67), which includes the screened potential. Fortunately, the newly obtained values were smaller, being of 18 Ha for ecut and 4 Ha for ecuteps, using the same 100 bands obtained before for the summation of this latter quantity (equation (2.47)). For the parameter ecutsigx, no convergence study was necessary, since this is the energy cut-off that it is used to calculate the exchange part of the self-energy (equation 2.50). The self-energy operator is not constructed by the software; the software does not correct the energy in the optical properties calculation for the points in the Brillouin zone. In this type of calculation, a rigid or scissors shift is selected, in order to approximate the behavior of the bands that were corrected by using the GWA (see equation (2.74), the quantities denoted as E^{QP}). The value for the scissors shift was of 1.52 eV, corresponding to the difference in

energy of the DFT band-gap value (transition Δ_1) and the GW band-gap value (transition Δ_4), presented in Table 3.3. It is important to say that this is just an approximation. The bands to be included in the summation of equation (2.74) are, ideally, the occupied valence and the corresponding unoccupied conduction bands. That is, the first ten bands, in the case of the blue phosphorene. As it can be seen in Figure 3.5, the transitions that are responsible of the resonance structure around the direct band gap in the optical response of blue phosphorene are not much affected in performing this approximation.

In this sense, the next convergence study was that of the bands to be included in the summation of the equation (2.74). Ideally, all the valence and conduction bands have to be included but with a convergence study only some bands can be used in order to calculate a converged spectrum. In Figure 3.6, spectra of the imaginary part of the parallel component of the dielectric function, for different number of valence and conduction bands are plotted. In ABINIT, for excitonic calculations, the parameter that sets the lower valence band included in the calculation is bs_loband while the parameter that defines the maximum conduction band to be included has the same parameter name nband as that used for the number of the bands in the sum for the self-energy operator in GW calculations. As a result, bs_loband was selected to be equal to 2 and nband equal to 10; this means that four valence bands and five conduction bands were considered in the calculation. For the cases of bs_loband $= 3$ and nband $= 8$, and bs_loband $= 3$ and nband $= 8$, a considerable change in the response is evident. For the cases of bs_loband $= 2$ and nband $= 9$, and bs_loband $= 2$ and nband $= 10$, just a small shift is present in the response, but the latter does not contain the unphysical behavior around 3 eV. A new case was necessary to determine that convergence was reached. The difference between bs_loband $= 1$ and nband $= 10$, and bs_loband $= 2$ and nband $= 10$ is minimal, so the latter was considered as the converged values for those parameters.

Next, the more demanding convergence study was performed, namely, the convergence with respect to the number of **k** points in the reciprocal space. The **k**-point grid was augmented gradually. Some of the obtained spectra are presented in Figure 3.7. The yellow spectra ($72 \times 72 \times 1$) shows a lot of peaks, indicating the low convergence value of the grid. For the blue spectra ($76 \times 76 \times 1$) this behavior is reduced and only seen between 5 and 6 eV. It can be noted that the purple spectra ($78 \times 78 \times 1$) it is well converged. For

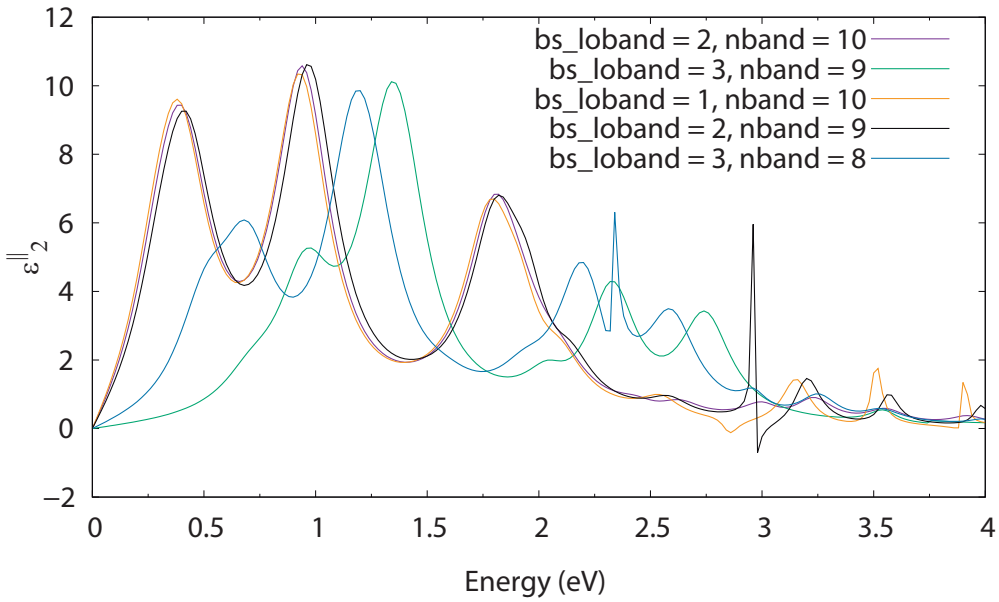

Figure 3.6: Spectra of the imaginary part of the in-plane component of the dielectric function calculated within the BSE formalism, for different values of bs_loband and nband. The purple or first graph was considered to be well converged, so four valence and five conduction bands were used in the calculations.

this latter, a total of 6084 points were necessary to reach the convergence.

A summary of the used convergence parameters values, obtained from the convergence tests is presented in Table 3.4, together with a comparison of respective data with other works. The calculated spectrum of the in-plane dielectric using the BSE formalism is shown in Figure 3.8. The real part has a static value $\epsilon_1^{||}(0)$ or DC value of 3.12. Also, $\epsilon_1^{||}$ reaches its maximum value of 9.12 at 3.94 eV. On the other hand, the imaginary part of the dielectric function $\epsilon_2^{||}$ has its maximum of 17.97 at its resonance frequency or at 4.03 eV . The resonance appears since in this specific frequency exist a maximum absorption of light, because the energy of the incident photons exactly match the direct transitions of the electrons in the material (see Figure 3.5). Similarly, some others peaks in the imaginary part of the dielectric function suggest that there exist some others transitions that are being match at that specific frequency value. Specially, the peak at 2.49 eV is the excitonic peak,

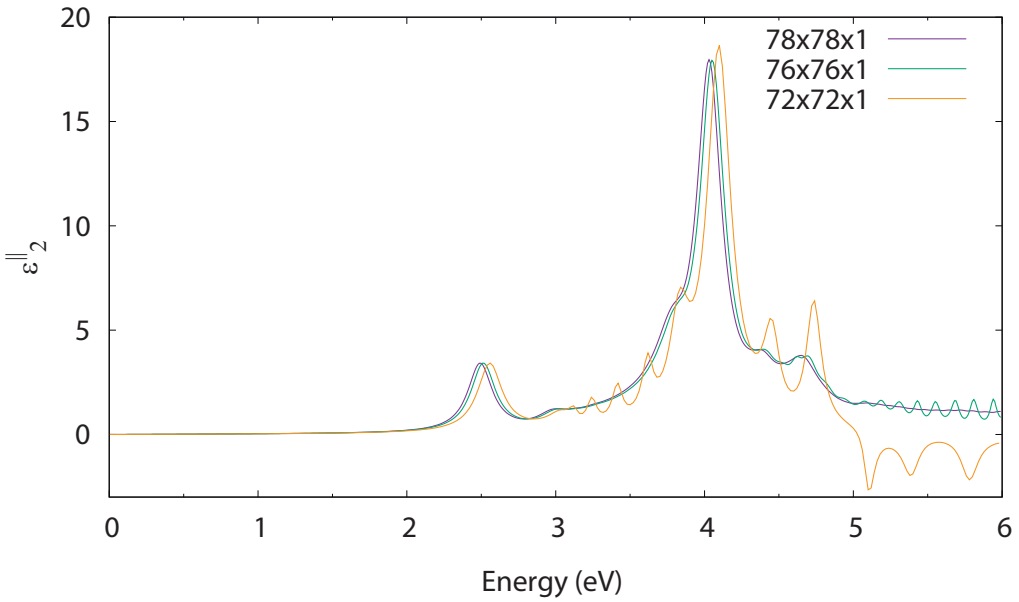

Figure 3.7: Spectra of the imaginary part of the in-plane component of the dielectric function calculated within the BSE formalism, for different values of the **k** points grid. The purple or first graph was considered to be well converged, so a grid of $78 \times 78 \times 1$ or a total of 6084 **k** points were considered in the calculation.

i.e. the energy at which the formation of excitons is at maximum, which results of excitonic absorption. The consequence that this have in $\epsilon_1^{||}$ is the peak value of 5.55 at 2.4 eV.

Table 3.4: Comparison of the convergence parameters obtained in this work to perform the excitonic calculations with those reported by other authors.

	ecut **(Ha)**	bs_loband	nband	ecuteps **(Ha)**	**k-point grid**	**Code**
This work	18	2	10	4	$78 \times 78 \times 1$	ABINIT
[88]						
[90]		3	8		$120 \times 120 \times 1$	BerkeleyGW [1]
[91]		2	9		$52 \times 52 \times 1$	BerkeleyGW
[92]		2	9		$42 \times 42 \times 1$	YAMBO [2]

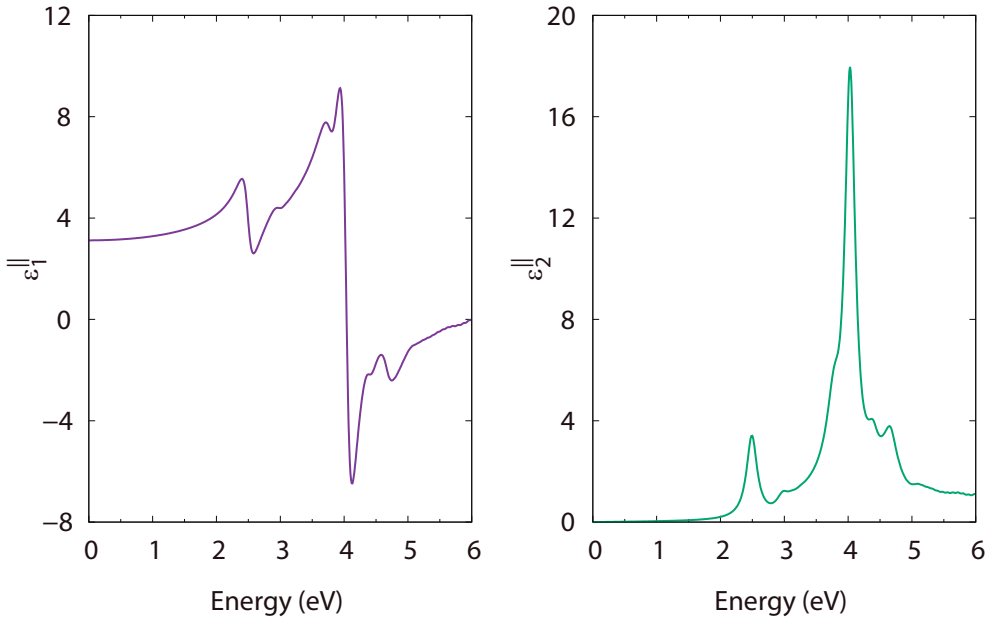

Figure 3.8: Spectra of the real (left) and imaginary (right) parts of the in-plane component of the dielectric function $\epsilon^{||}$ obtained within the Bethe-Salpeter formalism for the blue phosphorene.

From Figure 2.7 one can see that the independent-particle polarizability and the corresponding dielectric matrix is necessary to solve the BSE (step (3)). The corresponding spectrum for the dielectric function, calculated within the RPA, is shown in Figure 3.9. In this case, the absorption window is at aproximately 2 eV, which corresponds with the fundamental direct gap calculated within the Kohn-Sham approach. The imaginary part of the dielectric function has a maximum of 7.88 at the resonance frequency, located at 3.97 eV. The real part has a static value $\epsilon_1^{||}(0)$ of 3.04. Also, $\epsilon_1^{||}$ reaches its maximum value of 7.55 at 3.58 eV.

To demonstrate that the energy corrections within the GWA do not predict correctly the optical properties, the spectrum calculated within the RPA but using the quasiparticle energies corrections is shown in Figure 3.10. In this case, all the values are blue shifted 1.5 eV with respect to the independent-particle calculation (see Figure 3.9), which is the energy value used to shift

[1] https://berkeleygw.org/
[2] https://www.yambo-code.eu/

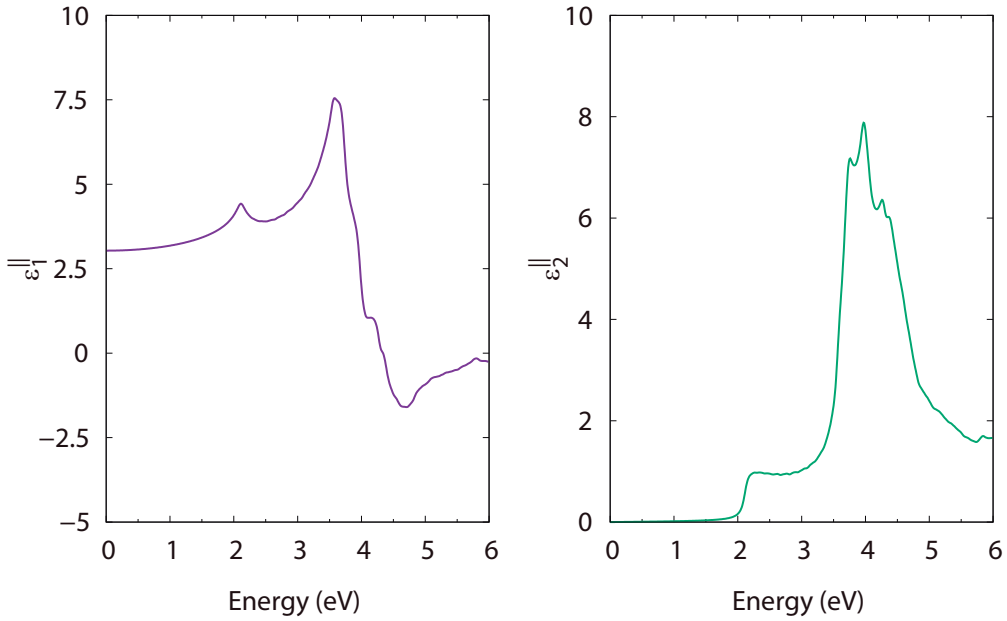

Figure 3.9: Spectra of the real (left) and imaginary (right) parts of the in-plane component of the dielectric function ($\epsilon^{||}$) obtained within the independent-particle approach and the RPA for the blue phosphorene.

all the bands in the calculation, as was explained before. The real part of the dielectric function has a static value of 2.5. Also, this real part reaches a maximum of 7.39 at 5.09 eV. On the other hand, the imaginary part of the dielectric function has a maximum of 7.88 at 5.47 eV.

The comparison between the spectra of the imaginary part of the in-plane component of the dielectric function $\epsilon^{||}$ calculated using the independent-particle approach, within the RPA, (RPA-KS), the dielectric function for which the quasiparticle energies where used, within the RPA (RPA-GW), and within the Bethe-Salpeter formalism (BS) is shown in Figure 3.11. Here is easy to see that neither the RPA-KS nor the RPA-GW calculated dielectric function could predict correctly the corresponding below-band-gap absorption. Also that these two are qualitatively the same, for this case, being the RPA-GW spectrum blue shifted with respect to the RPA-KS one. In general, BS curve compares well with other reported curves in that range of the spectrum, as that of Villegas *et. al.* [91] and İyikanat *et. al.* [92], showing the corresponding excitonic peak, at around 2.5 eV, and the resonance, at

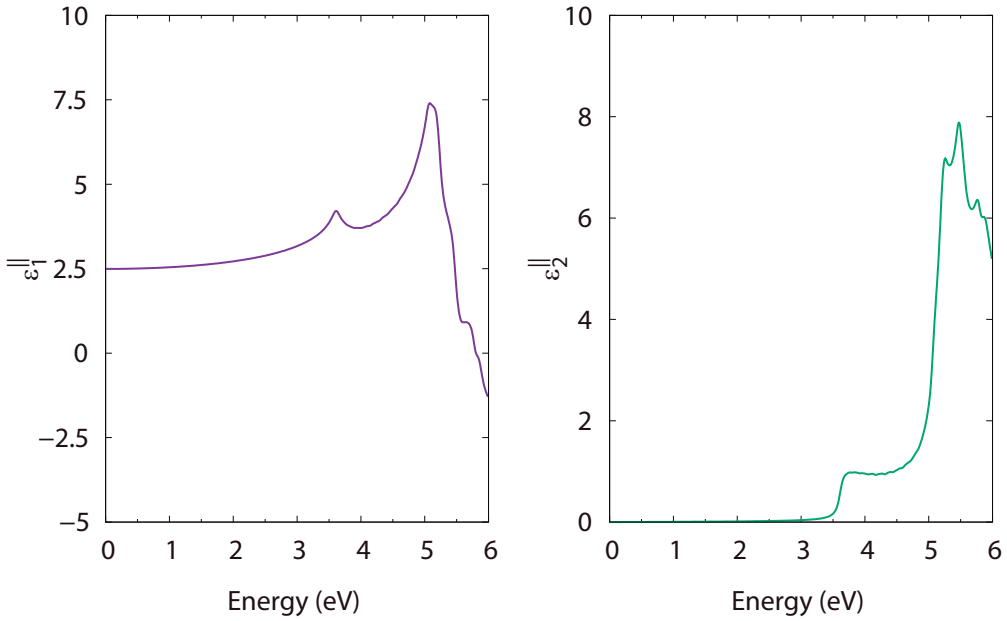

Figure 3.10: Spectra of the real (left) and imaginary (right) parts of the in-plane component of the dielectric function ($\epsilon^{||}$) obtained using the GW quasiparticle energies for the evaluation of the optical response within the RPA for the blue phosphorene.

around 4.1 eV.

Finally, a comparison of the spectra of the in-plane dielectric function calculated with different values of the broadening factor was made (see Figure 3.12). The broadening factor also acts as a damping factor in the evaluation of the optical response. If the broadening factor is zero then the imaginary part of the dielectric function at the resonance frequency will tend to infinity. If the value of the broadening factor is not zero, and increased, the peaks of ϵ_2 will be more damped. In general, the value of the broadening factor is of experimental interest, because it can be tuned to match the experimental curve and the theoretically predicted one.

The calculated spectrum of the in-plane dielectric using the BSE formalism, for a broadening value of 100 meV was shown in Figure 3.13. This was obtained by using the default value of the parameter used in ABINIT to considerer the broadening in the calculation of the Bethe-Salpeter spectrum,

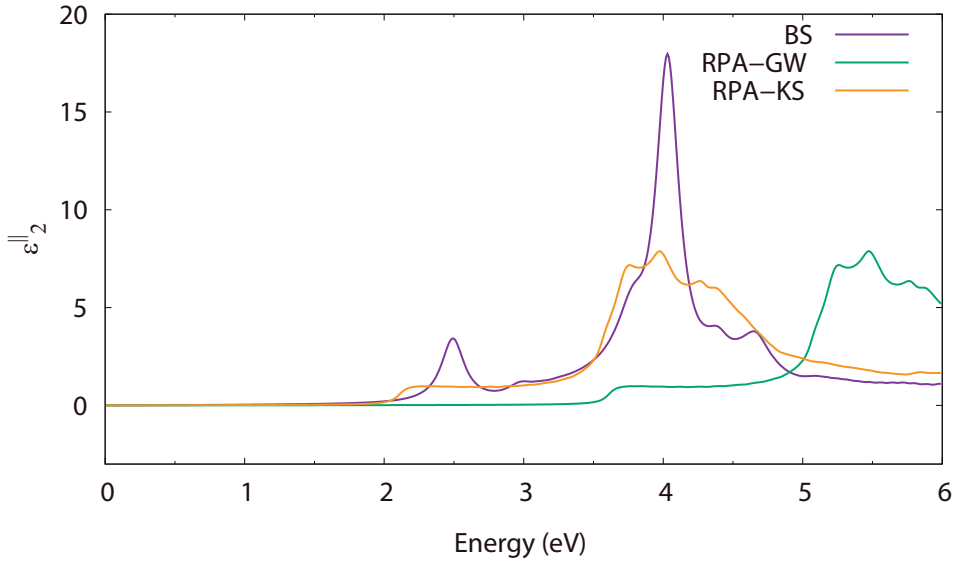

Figure 3.11: Spectra of the imaginary part of the in-plane component of the dielectric function ($\epsilon^{||}$) calculated within the Bethe-Salpeter formalism (BS), using the Kohn-Sham eigenvalues to obtain the polarizability (RPA-KS) and using the quasiparticle energies to obtain the polarizability (RPA-GW).

and is called zcut. The one calculated for a broadening factor of 50 meV is shown in Figure 3.13. This was considered in order to reproduce the results reported by Villegas *et. al.* [91], who did the calculation for the same spectrum range and considering that value of broadening factor. In our case, the real part has a static value of 3.12. Also, $\epsilon_1^{||}$ reaches its maximum value of 17.33 at 3.98 eV. The imaginary part of the dielectric function has its maximum value of 34.04 at 4.03 eV and the excitonic peak is still at 2.49 eV.

The calculated complex refractive index, corresponding to the dielectric function for a broadening of 50 meV, is presented in Figure 3.14. The real part of the refractive index $n^{||}$ has a static value of 1.77; it reaches its maximum value of 4.76 at 4 eV. The imaginary part of the refractive index or absorption coefficient $\kappa^{||}$ has its maximum value of 4.58 at 4.06 eV. The excitonic peak it is located at 2.51 eV and has a value of 1.44.

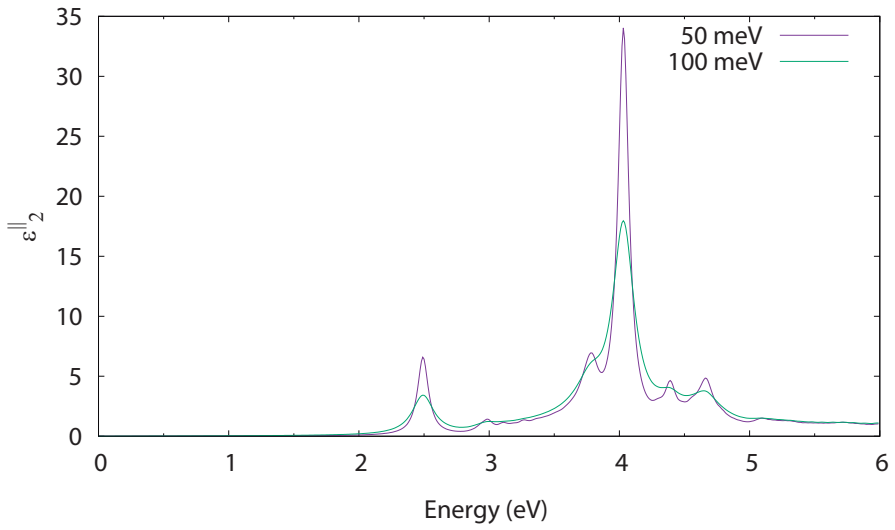

Figure 3.12: Spectra of the imaginary part of the in-plane component of the dielectric function calculated within the BSE formalism for different values of the broadening factor or the imaginary frequency.

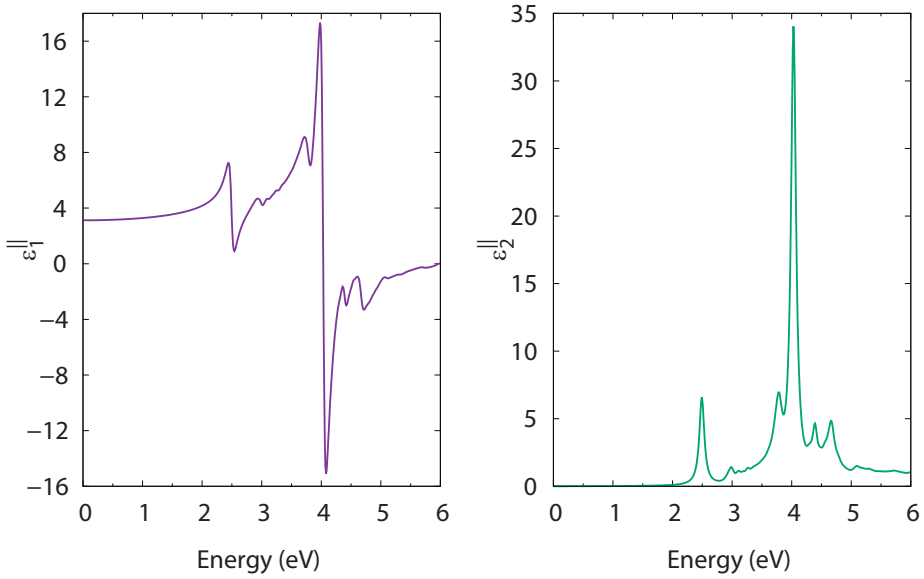

Figure 3.13: Spectra of the real (left) and imaginary (right) parts of the in-plane component of the dielectric function $\epsilon^{||}$ obtained within the Bethe-Salpeter formalism for the blue phosphorene, using a broadening of 50 meV.

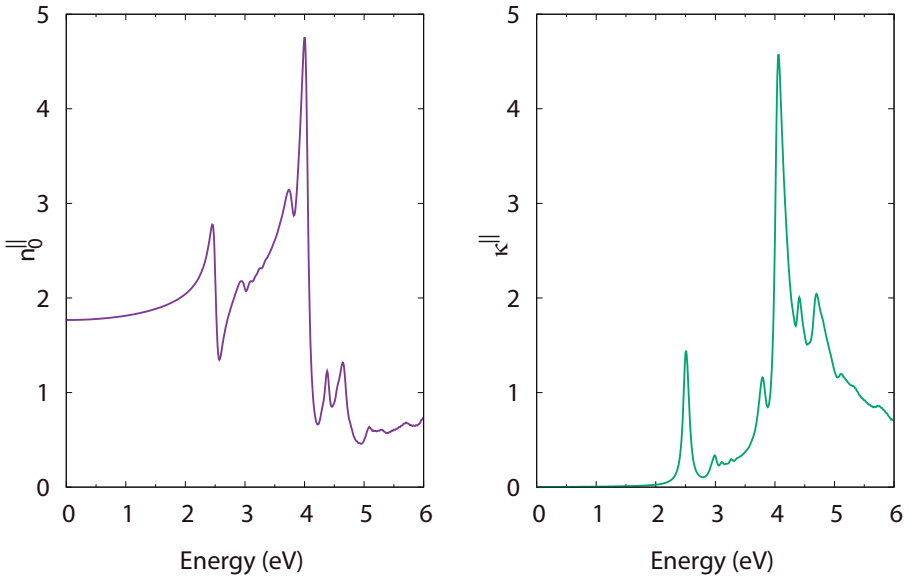

Figure 3.14: Spectra of the real (left) and imaginary (right) parts of the in-plane component of the complex index of refraction ($\hat{n}^{||}$) obtained within the Bethe-Salpeter formalism for the blue phosphorene, using a broadening of 50 meV.

Chapter 4

Conclusions

An exhaustive revision of the state of art of optical response studies of blue phosphorene, which consider the many-body effects, was made. The optimize crystalline structure of blue phosphorene was obtained from a previous work, where the structural parameters are in good agreement with those reported previously. The electronic band structure of blue phosphorene was obtained by using Density Functional Theory within the Generalized Gradient Approximation. The energy corrections to the bands were calculated in a specific set of **k** points within the irreducible Brillouin zone by employing the GW approximation. The complete quasiparticle band structure was determined by using maximally-localized Wannier functions and the corresponding interpolation scheme. The optical response including excitonic effects (electron-hole interactions) was calculated within the Bethe-Salpeter formalism. This excitonic spectrum was compared with both the independent-particle and GW optical response, showing that only the one calculated using the Bethe-Salpeter approach is able to predict below-band-gap absorption. In general, the proposed goals for the thesis were accomplished.

The quasiparticle band structure was of great importance in showing that, in general, this can not be calculated by obtaining the energy correction for just a one point in the reciprocal space and then applying a rigid shift to the DFT band structure. The usage of Wannier functions, with the aid of the Wannier90 software, is what enable us to obtain such a band structure, which could be impossible, or highly computationally demanding, without that formalism. Also, qualitatively, the behavior of the bands can be compared

with other works; the band-gap value is also well compared (of around 3.4 eV). It is easy to see that the converged values for the different paremeters used to perform the complete calculation are also in agreement.

For the excitonic spectrum, the comparison with previous works shows that the determined convergence parameters are, in general, very similar. By inspection, the spectrums of the cited works are comparable for both the excitonic peak (at around 2.5 eV) and the resonance frequency (of 4.1 eV), with those obtained in this one (2.49 and 4.03 eV).

The comparison among the excitonic spectrum, the RPA independent-particle approach and the RPA using the GW quasiparticle energies shows that the inclusion of the electron-hole interactions greatly changes the optical response, demostrating the importance of including these interactions in the optical properties calculations. The prediction of the below-band-gap absorption of the excitonic calculation could be compared with the experimental measumerents for semiconductors, which cannot be explained with the typical DFT calculation nor with the usage of the quasiparticle energies corrections to calculate the optical response, as was stated as hyphotesis for the development of this work.

As was mentioned before, the results were calculated using the ABINIT software exclusively, except for the Wannier interpolation scheme. The comparison between the other works shows that there is no big difference in performing this type of calculation using different softwares, even though the convergence values may change for the same system. This could be both related to the code implementation and the approximation that the software considers.

Finally, due to the developed work and thesis research, one can have a perspective of the new possible work that could be performed in order to continue in the 2D materials area. In general, the topological properties are one of the main research areas today, because material scientists are interested in predict properties that could be then measured on the laboratory. For this case, it is necessary to analize many of the new predicted 2D materials and to determine whether they could have this type of properties.

Also, many of the modern issues are that of the energy consumption and renewable energies; for that, many researchers are looking for new promizing materials that could be used in the development of the new generation of

photovoltaic devices. This new devices may have a greater portability and conversion rate of light than the actual ones, considering that they may have a "greener" impact. The 2D materials may play an important role in this topic, in which many has been studied but there still a path to road.

Appendix A

What is a functional?

A variational principle is one that enables a problem to be solved using calculus of variations, which concerns finding functions that optimize the values of quantities that depend on those functions [95]. Considering a function $F(x, y(x), y(x)')$ and the integral

$$I = \int_a^b F(x, y(x), y(x)')\, dx = I[y(x)], \tag{A.1}$$

such an integral is called a ***functional***. The prime notation on y denotes the first derivative with respect to x. It is a generalization of a function in that it is a number which depends on a function rather than on another number [95].

In finding which $y(x)$ makes the functional a maximum or a minimum requires that the following expression must be satisfied

$$\frac{\partial F}{\partial y} - \frac{d}{dx}\frac{\partial F}{\partial y'} = 0 \tag{A.2}$$

This is known as the variational or ***functional derivative*** of F with respect to y and is sometimes written as $\frac{\delta F}{\delta y}$. The equation A.2 is called the Euler-Lagrange equation. Many laws of physics may be stated in terms of a variational problem defining a functional, such as Hamilton's principle and Fermat's principle.

Appendix B

Wannier functions

The original work of Wannier [79] was intended to show that the description of the electrons in crystals can be that of the combination of the two different descriptions used in that time: running waves represented in the Bloch theorem and localized in space "atomic" functions.

The description of the theory behind Wannier functions, scope and software developed for the calculations of interpolated band structures using them is presented here.

In the independent-particle approximation, the electronic ground state of a system is determined by specifying a set of one-particle orbitals and their occupations. In atomic crystals, these one-particle orbitals are normally written as Bloch functions $\psi_{n\mathbf{k}}(\mathbf{r})$ characterized by a crystal momentum $\mathbf{k}$ lying inside the Brillouin zone and a band index n. However, alternative representations are possible, such as that of Wannier, defined by an unitary transformation from the Bloch functions to a set of localized Wannier functions (WFs). One feature of WFs is that, unlike Bloch functions, WFs are not eigenstates of the Hamiltonian; in selecting them, one trades off localization in energy for localization in space [96]. A second feature is that WFs are non-unique. This is a consequence of the phase indeterminacy that Bloch orbitals $\psi_{n\mathbf{k}}(\mathbf{r})$ have at every wavevector $\mathbf{k}$ or, more generally, the gauge indeterminacy of applying any arbitrary unitary transformation to the occupied Bloch states at each $\mathbf{k}$. This second indeterminacy is troublesome in the case of degeneracy of occupied bands at certain high symmetry points in the Brillouin

zone, making a partition into separate "bands", that could separately be transformed in Wannier functions, problematic [96]. Therefore, first a prior knowledge of the states to use to compute WFs is necessary. In this respect, Marzari and Vanderbilt introduced a "maximal localization" criterion for identifying a unique set of WFs for a given crystalline insulator [97]. Such development was the start for electronic structure community to construct maximally-localized WFs (MLWFs) explicitly.

B.1 General description

In the mathematical description, the one-particle effective Hamiltonian H commutes with the lattice-translation operator $T_{\mathbf{R}}$. This property lead to choose as common eigenstates the Bloch orbitals

$$\psi_{n\mathbf{k}}(\mathbf{r}) = u_{n\mathbf{k}}(\mathbf{r})e^{i\mathbf{k}\cdot\mathbf{r}}, \tag{B.1}$$

where $u_{n\mathbf{k}}(\mathbf{r})$ has the periodicity of the lattice.

Note that Bloch functions at different $\mathbf{k}$ have different envelope functions $e^{i\mathbf{k}\cdot\mathbf{r}}$. Hence, it can be possible to build a localized "wave packet" by superposing Bloch functions of different $\mathbf{k}$ as [96]

$$w_0(\mathbf{r}) = \frac{V}{(2\pi)^3}\int_{\mathrm{BZ}} d\mathbf{k}\psi_{n\mathbf{k}}(\mathbf{r}), \tag{B.2}$$

where V is the real space primitive cell volume and the integral is carried out over the Brillouin zone (BZ). Inserting a phase factor $e^{-i\mathbf{k}\cdot\mathbf{R}}$ into the integrand of equation B.2, where $\mathbf{R}$ is a real space lattice vector; this has the effect of translating the real space WF by $\mathbf{R}$, generating additional WFs. Hence, using Dirac notation WF's can be written as

$$|\mathbf{R}n\rangle = \frac{V}{(2\pi)^3}\int_{\mathrm{BZ}} d\mathbf{k}e^{-i\mathbf{k}\cdot\mathbf{R}}\,|\psi_{n\mathbf{k}}\rangle\,, \tag{B.3}$$

where $|\mathbf{R}n\rangle$ is the WF $w_{\mathbf{R}n}$ at position $\mathbf{R}$ and with a band index n. The set of functions $|\mathbf{R}n\rangle$ is orthonormal and equation B.3 takes the form of a Fourier transform. The corresponding inverse Fourier transform is

$$|\psi_{n\mathbf{k}}\rangle = \sum_{\mathbf{R}} e^{i\mathbf{k}\cdot\mathbf{R}}\,|\mathbf{R}n\rangle\,. \tag{B.4}$$

Most important, Bloch and Wannier states (equations (B.4 and (B.3)) provide an equally valid description of the band subspace, even if WFs are not not Hamiltonian eigenstates. This can be seen by expressing the band projection operator P in both representations [96]

$$P = \frac{V}{(2\pi)^3} \int_{\mathrm{BZ}} d\mathbf{k} \left|\psi_{n\mathbf{k}}\right\rangle \left\langle\psi_{n\mathbf{k}}\right| = \sum_{\mathbf{R}} \left|\mathbf{R}n\right\rangle \left\langle\mathbf{R}n\right|, \tag{B.5}$$

hence WFs represents the space spanned by Bloch band in a crystal, where they are characterized by being localized and having the same information that is contained in the Bloch functions.

The gauge freedom arises in the definition of Bloch state $\psi_{n\mathbf{k}}$ because

$$\left|\psi'_{n\mathbf{k}}\right\rangle = e^{i\phi_n(\mathbf{k})} \left|\psi_{n\mathbf{k}}\right\rangle, \tag{B.6}$$

where $\phi_n(\mathbf{k})$ is any real periodic function in reciprocal space. The gauge freedom given trough equation (B.6) gives a particular set of WFs; so different choices of gauge would give different sets of WFs having in general different shapes and spreads. In conclusion, WFs are strongly not unique so one would like to choose the "best" phase in terms of localization (to obtain the MLWF's). The criterion to determine that the WFs are maximally-localized, presented by Marzari and Vanderbilt [97], is that the second momentum or the spread calculated for a given set of WFs

$$\Omega = \sum_n [\left\langle w_{n\mathbf{0}}(\mathbf{r})\right| \mathbf{r}^2 \left|w_{n\mathbf{0}}(\mathbf{r})\right\rangle - (\left\langle w_{n\mathbf{0}}(\mathbf{r})\right| \mathbf{r} \left|w_{n\mathbf{0}}(\mathbf{r})\right\rangle)^2] \tag{B.7}$$

is a minimum. One have to take into account that some of the terms of equation B.7 are gauge invariant, so the total spread could not ever be zero.

B.2 Quasiparticle band structure calculation

WFs can be generated by using the Kohn-Sham Bloch functions and eigenvalues calculated with the formalism of DFT. The disadvantage is that the calculation of the Kohn-Sham energy bands underestimate the energy band gaps of insulators and semiconductors. These energy bands can be corrected using many-body perturbation theory within the GW approximation [96]. However, one practical difficulty in generating the GW band structure is

that the evaluation of quasiparticle corrections to eigenenergies along different symmetry lines in the Brillouin zone is computationally very demanding. One numerical approximation is to perform the GW calculation only at selected high-symmetry $\mathbf{k}$ points, and then deduce a "scissors correction," i.e., a constant shift to be applied to the conduction-band Kohn-Sham eigenvalues elsewhere in the Brillouin zone [96]. In 2009 Hamann and Vanderbilt [98], proposed a method using Wannier interpolation to determine the GW quasiparticle bands efficiently and accurately at arbitrary $\mathbf{k}$ points in the Brillouin zone. Wannier interpolation schemes, by which quantities computed on a relatively coarse $\mathbf{k}$-space mesh can be used to interpolate faithfully onto an arbitrarily fine $\mathbf{k}$-space mesh, are relatively low cost. In this case, the computed energy corrections are determined for a relatively coarse mesh and, after the interpolation, the complete quasiparticle band structure can be obtained.

Once we have obtained the MLWF's for a group of bands, a set of Bloch-like states can be constructed

$$\left|\psi'_{n\mathbf{k}}\right\rangle = \sum_{\mathbf{R}} e^{i\mathbf{k}\cdot\mathbf{R}} \left|\mathbf{R}n\right\rangle . \tag{B.8}$$

The prime serves as a reminder that the states $\left|\psi'_{n\mathbf{k}}\right\rangle$ are generally not eigenstates of the Hamiltonian [1]. At a given $\mathbf{k}$, the Hamiltonian matrix elements in the space of the bands is represented by the matrix

$$H'_{\mathbf{k},nm} = \left\langle \psi'_{n\mathbf{k}} \right| H \left| \psi'_{m\mathbf{k}} \right\rangle = \sum_{\mathbf{R}} e^{i\mathbf{k}\cdot\mathbf{R}} \left\langle \mathbf{0}n \right| H \left|\mathbf{R}m\right\rangle . \tag{B.9}$$

In general this is a non-diagonal matrix in the band-like indices, and the interpolated eigenenergies are obtained by diagonalization,

$$H^H_{\mathbf{k},nm} = \left[U^\dagger_{\mathbf{k}} H_{\mathbf{k}} U_{\mathbf{k}}\right]_{nm} = \delta_{nm}\epsilon_{n\mathbf{k}}, \tag{B.10}$$

where the unitary matrices $U_{\mathbf{k}}$ transform between the Wannier and Hamiltonian gauge [2] (denoted by the H index) and $\epsilon_{n\mathbf{k}}$ are the energy eigenvalues at a given $\mathbf{k}$. If we insert into equations (B.9) and (B.10) a $\mathbf{k}$ at which the GW corrections were determined, we simply recover the eigenvalues $\epsilon_{n\mathbf{k}}$, while for arbitrary $\mathbf{k}$ the resulting $\bar{\epsilon}_{n\mathbf{k}}$ interpolate smoothly between the values of the grid.

[1] These states belong to the *Wannier gauge*.

[2] The gauge in which the Hamiltonian is diagonal.

B.3 The Wannier90 software

In order to exploit the WFs theory in real calculations one can use Wannier90, an open-source code for generating MLWF's [99]. It allows to compute electronic properties of materials with high efficiency and accuracy. ABINIT has an interface to Wannier90 and there are several post-processing codes that are able to use the output of Wannier90 for further analysis and calculations.

More information about the software, tutorials and general documentation can be found on the official website http://www.wannier.org/.

Appendix C

The ABINIT software

"ABINIT is a package whose main program allows one to find the total energy, charge density and electronic structure of systems made of electrons and nuclei (molecules and periodic solids) within Density Functional Theory (DFT), using pseudopotentials and a planewave basis. ABINIT also optimizes the geometry according to the DFT forces and stresses, or performs molecular dynamics simulations using these forces, or generates phonons, Born effective charges, and dielectric tensors, based on Density-Functional Perturbation Theory, and many more properties. Excited states and spectra can be computed within the Many-Body Perturbation Theory (the GW approximation and the Bethe-Salpeter equation). DFT+U and Dynamical mean-field theory are available for strongly correlated materials. In addition to the main ABINIT code, different utility programs are provided"[100–102].

ABINIT is distributed under the GNU General Public Licence. It is fully documented: it has an user guide, installation tutorials, lists of variables, a public forum for the users to ask questions, a large pseudopotential library and various tutorials to learn how to use the code. For more related information, updates and improvements, visit the official web site: https://www.abinit.org/.

Bibliography

1. Planck, M. On the theory of the energy distribution law of the normal spectrum. *Verh. Deut. Phys. Ges* **2,** 237–245 (1900).
2. Einstein, A. On a heuristic point of view concerning the production and transformation of light. *Annalen der Physik,* 1–18 (1905).
3. Bohr, N. I. On the constitution of atoms and molecules. *The London, Edinburgh, and Dublin Philosophical Magazine and Journal of Science* **26,** 1–25 (1913).
4. Bohr, N. II. On the constitution of atoms and molecules. *The London, Edinburgh, and Dublin Philosophical Magazine and Journal of Science* **26,** 476–502 (1913).
5. Bohr, N. III. On the constitution of atoms and molecules. *The London, Edinburgh, and Dublin Philosophical Magazine and Journal of Science* **26,** 857–875 (1913).
6. De Broglie, L. *Recherches sur la theorie des quanta.* PhD thesis (Univ. de Paris., 1924).
7. Heisenberg, W. Quantum-theoretical re-interpretation of kinematic and mechanical relations. *Z. Phys* **33,** 879–893 (1925).
8. Born, M. & Jordan, P. Zur quantenmechanik. *Zeitschrift für Physik* **34,** 858–888 (1925).
9. Born, M., Heisenberg, W. & Jordan, P. Zur Quantenmechanik. II. *Zeitsc-hrift für Physik* **35,** 557–615 (1926).
10. Schrödinger, E. An undulatory theory of the mechanics of atoms and molecules. *Physical Review* **28,** 1049 (1926).
11. Kuhn, T. S. *The structure of scientific revolutions* (Chicago University of Chicago Press, 1970).
12. Bloch, F. Quantum mechanics of electrons in crystal lattices. *Z. Phys* **52,** 555–600 (1928).

13. Wilson, A. H. The theory of electronic semi-conductors I. *Proceedings of the Royal Society of London.* **133,** 458–491 (1931).
14. Brillouin, L. Les électrons libres dans les métaux et le role des réflexions de Bragg. *J. Phys. Radium* **1,** 377–400 (1930).
15. Kronig, R. d. L. & Penney, W. G. Quantum mechanics of electrons in crystal lattices. *Proceedings of the royal society of London.* **130,** 499–513 (1931).
16. Dirac, P. A. M. Quantum mechanics of many-electron systems. *Proceedings of the Royal Society of London.* **123,** 714–733 (1929).
17. Wigner, E. On the interaction of electrons in metals. *Physical Review* **46,** 1002 (1934).
18. Thomas, L. H. *The calculation of atomic fields* in *Mathematical proceedings of the Cambridge philosophical society* **23** (1927), 542–548.
19. Fermi, E. Un metodo statistico per la determinazione di alcune priorieta dell'atome. *Rend. Accad. Naz. Lincei* **6,** 32 (1927).
20. Dirac, P. A. *Note on exchange phenomena in the Thomas atom* in *Mathematical proceedings of the Cambridge philosophical society* **26** (1930), 376–385.
21. Hartree, D. R. *The wave mechanics of an atom with a non-Coulomb central field. Part I. Theory and methods* in *Mathematical Proceedings of the Cambridge Philosophical Society* **24** (1928), 89–110.
22. Hartree, D. R. *The wave mechanics of an atom with a non-coulomb central field. Part II. Some results and discussion* in *Mathematical Proceedings of the Cambridge Philosophical Society* **24** (1928), 111–132.
23. Fock, V. Näherungsmethode zur Lösung des quantenmechanischen Mehrkörperproblems. *Zeitschrift für Physik* **61,** 126–148 (1930).
24. Hohenberg, P. & Kohn, W. Inhomogeneous electron gas. *Phys. Rev* **136,** B864 (1964).
25. Kohn, W. & Sham, L. J. Self-consistent equations including exchange and correlation effects. *Physical Review* **140,** A1133 (1965).
26. An, J. *et al.* Perspectives of 2D materials for optoelectronic integration. *Advanced Functional Materials* **32,** 2110119 (2022).
27. Novoselov, K. S. *et al.* Electric field effect in atomically thin carbon films. *Science* **306,** 666–669 (2004).
28. Novoselov, K. S. *et al.* Two-dimensional atomic crystals. *Proceedings of the National Academy of Sciences* **102,** 10451–10453 (2005).

29. Novoselov, K. S. *et al.* Two-dimensional gas of massless Dirac fermions in graphene. *Nature* **438,** 197–200 (2005).
30. Dresselhaus, M. S. & Dresselhaus, G. Intercalation compounds of graphite. *Advances in Physics* **51,** 1–186 (2002).
31. Ariel, V. & Natan, A. *Electron effective mass in graphene* in *2013 international conference on electromagnetics in advanced applications (ICEAA)* (2013), 696–698.
32. Kuc, A. Low-dimensional transition-metal dichalcogenides (2014).
33. Pakdel, A., Bando, Y. & Golberg, D. Nano boron nitride flatland. *Chemical Society Reviews* **43,** 934–959 (2014).
34. Liu, H., Neal, A. T., Zhu, Z., Tomanek, D. & Ye, P. D. Phosphorene: a new 2D material with high carrier mobility. *arXiv preprint arXiv:1401.4133* (2014).
35. Anichini, C. *et al.* Chemical sensing with 2D materials. *Chemical Society Reviews* **47,** 4860–4908 (2018).
36. You, J., Bongu, S., Bao, Q. & Panoiu, N. Nonlinear optical properties and applications of 2D materials: theoretical and experimental aspects. *Nanophotonics* **8,** 63–97 (2019).
37. Das, S., Pandey, D., Thomas, J. & Roy, T. The role of graphene and other 2D materials in solar photovoltaics. *Advanced Materials* **31,** 18027–22 (2019).
38. Liu, X. & Hersam, M. C. 2D materials for quantum information science. *Nature Reviews Materials* **4,** 669–684 (2019).
39. Thurn, H. & Kerbs, H. Crystal structure of violet phosphorus. *Angewandte Chemie International Edition in English* **5,** 1047–1048 (1966).
40. Hultgren, R., Gingrich, N. & Warren, B. The atomic distribution in red and black phosphorus and the crystal structure of black phosphorus. *The Journal of Chemical Physics* **3,** 351–355 (1935).
41. Zhu, Z. & Tománek, D. Semiconducting layered blue phosphorus: a computational study. *Physical Review Letters* **112,** 176802 (2014).
42. Dai, J. & Zeng, X. C. Bilayer phosphorene: effect of stacking order on bandgap and its potential applications in thin-film solar cells. *The Journal of Physical Chemistry Letters* **5,** 1289–1293 (2014).
43. Boulfelfel, S. E., Seifert, G., Grin, Y. & Leoni, S. Squeezing lone pairs: The A 17 to A 7 pressure-induced phase transition in black phosphorus. *Physical Review B* **85,** 014110 (2012).

44. Aierken, Y., Çakır, D., Sevik, C. & Peeters, F. M. Thermal properties of black and blue phosphorenes from a first-principles quasiharmonic approach. *Physical Review B* **92,** 081408 (2015).
45. Jain, A. & McGaughey, A. J. Strongly anisotropic in-plane thermal transport in single-layer black phosphorene. *Scientific Reports* **5,** 8501 (2015).
46. Ospina, D., Duque, C., Correa, J. & Morell, E. S. Twisted bilayer blue phosphorene: A direct band gap semiconductor. *Superlattices and Microstructures* **97,** 562–568 (2016).
47. Zhang, J. L. *et al.* Epitaxial growth of single layer blue phosphorus: a new phase of two-dimensional phosphorus. *Nano Letters* **16,** 4903–4908 (2016).
48. Ribeiro-Soares, J., Almeida, R., Cançado, L. G., Dresselhaus, M. S. & Jorio, A. Group theory for structural analysis and lattice vibrations in phosphorene systems. *Physical Review B* **91,** 205421 (2015).
49. Nava, J. J. *Estudio de las propiedades ópticas del fosforeno azul* Bachelor's Thesis (Universidad Autónoma de Baja California, Blvd. Benito Juárez S/N CP 21280, Mexicali, B.C. Mexico, Nov. 2020).
50. Xu, J.-P. *et al.* One-dimensional phosphorus chain and two-dimensional blue phosphorene grown on Au (111) by molecular-beam epitaxy. *Physical Review Materials* **1,** 061002 (2017).
51. Gu, C. *et al.* Growth of quasi-free-standing single-layer blue phosphorus on tellurium monolayer functionalized Au (111). *ACS Nano* **11,** 4943–4949 (2017).
52. Peng, Q., Wang, Z., Sa, B., Wu, B. & Sun, Z. Electronic structures and enhanced optical properties of blue phosphorene/transition metal dichalcogenides van der Waals heterostructures. *Scientific Reports* **6,** 31994 (2016).
53. Wang, B.-J. *et al.* Blue phosphorus/Mg(OH)2 van der Waals heterostructures as promising visible-light photocatalysts for water splitting. *The Journal of Physical Chemistry C* **122,** 7075–7080 (2018).
54. Sun, M., Wang, S., Yu, J. & Tang, W. Hydrogenated and halogenated blue phosphorene as Dirac materials: A first principles study. *Applied Surface Science* **392,** 46–50 (2017).
55. Ghosh, B., Nahas, S., Bhowmick, S. & Agarwal, A. Electric field induced gap modification in ultrathin blue phosphorus. *Physical Review B* **91,** 115433 (2015).

56. Huang, L. & Li, J. Tunable electronic structure of black phosphorus/blue phosphorus van der Waals pn heterostructure. *Applied Physics Letters* **108,** 083101 (2016).
57. Zhu, J., Zhang, J. & Hao, Y. Tunable schottky barrier in blue phosphorus-graphene heterojunction with normal strain. *Japanese Journal of Applied Physics* **55,** 080306 (2016).
58. Liu, N. & Zhou, S. Gas adsorption on monolayer blue phosphorus: implications for environmental stability and gas sensors. *Nanotechnology* **28,** 175708 (2017).
59. Li, Q.-F., Duan, C.-G., Wan, X. & Kuo, J.-L. Theoretical prediction of anode materials in Li-ion batteries on layered black and blue phosphorus. *The Journal of Physical Chemistry C* **119,** 8662–8670 (2015).
60. Sun, H., Liu, G., Li, Q. & Wan, X. First-principles study of thermal expansion and thermomechanics of single-layer black and blue phosphorus. *Physics Letters A* **380,** 2098–2104 (2016).
61. Martin, R. M. *Electronic structure: basic theory and practical methods* (Cambridge University Press, 2004).
62. Payne, M. C., Teter, M. P., Allan, D. C., Arias, T. & Joannopoulos, a. J. Iterative minimization techniques for ab initio total-energy calculations: molecular dynamics and conjugate gradients. *Reviews of Modern Physics* **64,** 1045 (1992).
63. Kittel, C. *Introduction to Solid State Physics* (John Wiley and Sons, 2005).
64. Harrison, W. A. *Electronic structure and the properties of solids: the physics of the chemical bond* (Dover Publications, Inc., 1989).
65. De La Peña, L. *Introducción a la mecánica cuántica* (Fondo de Cultura económica, 2006).
66. Sharma, S. & Ambrosch-Draxl, C. Second-Harmonic Optical Response from First Principles. *Physica Scripta* **T109,** 128. ISSN: 0031-8949 (2004).
67. Burke, K. & Wagner, L. O. DFT in a nutshell. *International Journal of Quantum Chemistry* **113,** 96–101 (2013).
68. Grumet, M., Liu, P., Kaltak, M., Klimeš, J. & Kresse, G. Beyond the quasiparticle approximation: Fully self-consistent G W calculations. *Physical Review B* **98,** 155143 (2018).
69. Hedin, L. New method for calculating the one-particle Green's function with application to the electron-gas problem. *Physical Review* **139,** A796 (1965).

70. Aulbur, W. G., Jönsson, L. & Wilkins, J. W. in (eds Ehrenreich, H. & Spaepen, F.) 1–218 (Academic Press, 2000).
71. Wen, X.-G. *Quantum field theory of many-body systems: from the origin of sound to an origin of light and electrons* (OUP Oxford, 2004).
72. Onida, G., Reining, L. & Rubio, A. Electronic excitations: density-functional versus many-body Green's-function approaches. *Reviews of Modern Physics* **74,** 601 (2002).
73. Fetter, A. L. & Walecka, J. D. *Quantum theory of many-particle systems* (Dover Publications, INC, 2003).
74. Weinberg, S. *The quantum theory of fields* (Cambridge university press, 1995).
75. Aryasetiawan, F. & Gunnarsson, O. The GW method. *Reports on Progress in Physics* **61,** 237 (1998).
76. Kaplan, T. The chemical potential. *Journal of Statistical Physics* **122,** 1237–1260 (2006).
77. Van Setten, M., Giantomassi, M., Gonze, X., Rignanese, G.-M. & Hautier, G. Automation methodologies and large-scale validation for GW: Towards high-throughput GW calculations. *Physical Review B* **96,** 155207 (2017).
78. Frenkel, J. On the transformation of light into heat in solids. II. *Physical Review* **37,** 1276 (1931).
79. Wannier, G. H. The Structure of Electronic Excitation Levels in Insulating Crystals. *Physical Review* **52,** 191 (1937).
80. Salpeter, E. E. & Bethe, H. A. A relativistic equation for bound-state problems. *Physical Review* **84,** 1232 (1951).
81. Rohlfing, M. & Louie, S. G. Electron-hole excitations and optical spectra from first principles. *Physical Review B* **62,** 4927 (2000).
82. Del Sole, R. & Fiorino, E. Macroscopic dielectric tensor at crystal surfaces. *Physical Review B* **29,** 4631 (1984).
83. Monkhorst, H. J. & Pack, J. D. Special points for Brillouin-zone integrations. *Physical Review B* **13,** 5188 (1976).
84. Pack, J. D. & Monkhorst, H. J. " Special points for Brillouin-zone integrations"—a reply. *Physical Review B* **16,** 1748 (1977).
85. Xiao, J. *et al.* Electronic structures and carrier mobilities of blue phosphorus nanoribbons and nanotubes: a first-principles study. *The Journal of Physical Chemistry C* **120,** 4638–4646 (2016).

86. Mogulkoc, Y., Modarresi, M., Mogulkoc, A. & Ciftci, Y. Electronic and optical properties of bilayer blue phosphorus. *Computational Materials Science* **124,** 23–29 (2016).
87. Pontes, R. B., Miwa, R. H., da Silva, A. J., Fazzio, A. & Padilha, J. E. Layer-dependent band alignment of few layers of blue phosphorus and their van der Waals heterostructures with graphene. *Physical Review B* **97,** 235419 (2018).
88. Galicia Hernandez, J. M., Fernandez-Escamilla, H., Guerrero Sanchez, J. & Takeuchi, N. Electronic and optical properties of the buckled and puckered phases of phosphorene and arsenene. *Scientific Reports* **12,** 1–14 (2022).
89. Han, W. H., Kim, S., Lee, I.-H. & Chang, K. J. Prediction of green phosphorus with tunable direct band gap and high mobility. *The Journal of Physical Chemistry Letters* **8,** 4627–4632 (2017).
90. Zhou, J., Cai, T.-Y. & Ju, S. Unusual Strain Dependence of Quasiparticle Electronic Structure, Exciton, and Optical Properties in Blue Phosphorene. *Physical Review Applied* **15,** 024045 (2021).
91. Villegas, C. E., Rodin, A., Carvalho, A. & Rocha, A. Two-dimensional exciton properties in monolayer semiconducting phosphorus allotropes. *Physical Chemistry Chemical Physics* **18,** 27829–27836 (2016).
92. İyikanat, F., Torun, E., Senger, R. T. & Sahin, H. Stacking-dependent excitonic properties of bilayer blue phosphorene. *Physical Review B* **100,** 125423 (2019).
93. Zhu, B. *et al.* Thermoelectric effect and devices on IVA and VA Xenes. *InfoMat* **3,** 271–292 (2021).
94. Yates, J. *Wannier90 A brief overview of the code* 2017. https://www.tcm.phy.cam.ac.uk/~jry20/ctut.pdf.
95. Mathews, J. & Walker, R. L. *Mathematical Methods of Physics* (WA Benjamin New York, 1970).
96. Marzari, N., Mostofi, A. A., Yates, J. R., Souza, I. & Vanderbilt, D. Maximally localized Wannier functions: Theory and applications. *Reviews of Modern Physics* **84,** 1419 (2012).
97. Marzari, N. & Vanderbilt, D. Maximally localized generalized Wannier functions for composite energy bands. *Physical Review B* **56,** 12847 (1997).
98. Hamann, D. & Vanderbilt, D. Maximally localized Wannier functions for GW quasiparticles. *Physical Review B* **79,** 045109 (2009).

99. Pizzi, G. *et al.* Wannier90 as a community code: new features and applications. *Journal of Physics: Condensed Matter* **32,** 165902 (2020).
100. Gonze, X. *et al.* The Abinit project: Impact, environment and recent developments. *Computer Physics Communication* **248,** 107042 (2020).
101. Romero, A. H. *et al.* ABINIT: Overview, and focus on selected capabilities. *Journal of Chemical Physics* **152,** 124102 (2020).
102. Gonze, X. First-principles responses of solids to atomic displacements and homogeneous electric fields: Implementation of a conjugate-gradient algorithm. *Physical Review B* **55,** 10337–10354. ISSN: 0163-1829, 1095-3795 (1997).
103. Bruneval, F., Vast, N. & Reining, L. Effect of self-consistency on quasiparticles in solids. *Physical Review B* **74,** 045102. ISSN: 1098-0121, 1550-235X (2006).